International Journal of Nanoscience and Nanoengineering
2018; 4(3): 35-56
http://www.openscienceonline.com/journal/nano

Critical Heat Flux Enhancement Using Nanofluids and Hybrid Nanofluids: A Review

Jason Bolton[1], Lande Liu[1, *], Jonathan Andrew Hinks[2], John Chee Chai[2]

[1]School of Applied Sciences, University of Huddersfield, Huddersfield, UK

[2]School of Computing and Engineering, University of Huddersfield, Huddersfield, UK

Email address

l.liu@hud.ac.u (L. Liu)

[*]Corresponding author

To cite this article

Jason Bolton, Lande Liu, Jonathan Andrew Hinks, John Chee Chai. Critical Heat Flux Enhancement Using Nanofluids and Hybrid Nanofluids: A Review. *International Journal of Nanoscience and Nanoengineering.* Vol. 4, No. 3, 2018, pp. 35-56.

Received: May 29, 2018; **Accepted**: July 3, 2018; **Published**: August 10, 2018

Abstract

Due to the significantly enhanced thermal properties of nanofluids, a considerably large amount of research has been performed to further develop this heat transfer medium. Not only has research been carried out in homogeneous suspensions of nanoparticles but research into the effectiveness of hybrid nanofluids has also been conducted. It has been observed experimentally that the critical heat flux (CHF) can also be enhanced by having low volume concentrations of nanoparticles in suspension. An up to 700% for hybrid opposed to up to 300% for having non-hybrid nanoparticles have been reported. This review covers the models used to predict the enhancements of thermal conductivity and convective heat transfer coefficient. Moreover, the main focus is given to the CHF enhancement with the possible mechanisms and explanations proposed for such an enhancement. Nanoparticles' deposition onto the heating surface together with the contact angle reduction and capillary wicking are thought to be the underlying causes for CHF enhancement. The Zuber correlation and Kandllikar's model have been found to be able to describe some experimental CHE enhancement data reasonably well. Onto the stability issue, among the three commonly used methods: chemical stabilisation, polymer stabilisation and sonication, it is thought that the chemical approach is favored as it is less affected by the operating and environmental conditions. Towards potential industrial applications, quantitative understanding of the enhancement mechanisms and maintaining long period of stability together with real time characterisation techniques of nanoparticles in fluids are thought to still remain as the main obstacles lying ahead to be addressed, and indeed, these are still the real challenges.

Keywords

Critical Heat Flux, Heat Transfer, Heat Transfer Enhancement, Nanofluids, Nanoparticles

1. Introduction

'Nanofluids' was a term first used by Choi in a conference paper in 1995 when proposing a way to enhance the thermal conductivity of a fluid by using nanoparticles. In the paper it was noted that as the nanoparticles have a significantly higher thermal conductivity than the fluid, it was possible to enhance the thermal conductivity of a fluid by dispersing particles between 1 nm and 100 nm in at least one principal dimension throughout a base fluid [1]. Alongside the enhancement in the thermal conductivity of the base fluid, it was found that the addition of nanoparticles also altered the viscosity and other thermal properties of the base fluid which led nanofluids to become a promising material to enhance the efficiency of heat transfer systems. Various nanoparticles and base fluids have been used; some of the most commonly researched nanoparticles are CuO, Al_2O_3, SiO_2 and TiO_2. Carbon nanotubes (CNTs), multi-walled carbon nanotubes (MWCNTs) and graphene-based nanofluids have become more prominent in recent research. Alongside the continuous study of homogeneous nanofluids, research into the effectiveness of hybrid nanofluids is also on the rise, with

some studies reporting heat transfer enhancements of up to 700% using a CNT hybrid nanofluid [2].

The production of nanofluids is normally carried out by a one-step or two-step process. In the one-step production process, the nanoparticles are directly produced in the base fluid whilst the nanoparticles are produced separately before being dispersed throughout the fluid in the two-step process. Several one-step production methods have been used, one of them being vacuum evaporation to directly produce nanofluids which was first developed by Akoh et al. [3] to determine the magnetic properties of ferrofluids, two other methods are laser ablation and chemical synthesis [4, 5].

There are two broad classes of techniques to characterise nanofluids. The first characterises the dimensions of the nanoparticles while the second determines the stability of the nanofluids which will be discussed in Section 4.

Transmission Electron Microscopy (TEM), Scanning Electron Microscopy (SEM), X-Ray Diffraction (XRD), and Dynamic Light Scattering (DLS) are some experimental techniques used to characterise the nanoparticles in nanofluids and hybrid nanofluids. They can be used to determine the shape, morphology, crystal structure and particle sizes of the nanoparticles.

Fourier Transform Infra-Red Spectroscopy (FT-IR), Thermogravimetric Analysis (TGA), Zeta potential analysis, Field Emission SEM (FE-SEM), Energy Dispersion Spectroscopy (EDS) and Raman Spectroscopy can be used to determine the thermal stability of the nanoparticles and the group surface chemistry [6]. Fluids with magnetic properties may be characterised by Vibration Sample Magnetometry (VSM) [5-8]. Other less common characterisation techniques such as Energy Dispersive (ED-XRD), X-ray powder diffraction (XRD), Boehm's titration and N_2 adsorption-desorption were used by Moghaddam et al. to determine the morphology and structure of a graphene-glycerol nanofluid [9].

2. Thermal Properties

Since the study of nanofluids began there has been a main focus on the enhanced thermophysical properties that could be achieved by adding a metallic substance to a fluid. With the addition of a different material such as SiO_2, Cu, Al_2O_3 or other materials with a high thermal conductance, a higher density and different rheological properties, it was thought that the average properties of a fluid would be considerably different. This led to a significant amount of study in hopes of developing models which explain the change in these properties, the main properties of focus were the thermal conductivity, viscosity, density and specific heat capacity of the now multi-phase fluid. Nevertheless, this review focuses on thermal property enhancement in particular the models.

2.1. Thermal Conductivity

A common method of measuring the thermal conductivity of a fluid is to use the transient hot wire (THW) method. In this approach, a wire of known initial resistance is submerged in a fluid, an electrical pulse is then passed through the wire dissipating the heat throughout the fluid, allowing the thermal conductivity to be calculated from the increase in the observed temperature [5, 10]. Other methods such as the transient plane source (TPS) technique which utilises a thermal constants analyser (TCA) to measure the thermal conductivity of a nanofluid can also be used. Further details on the setup of these procedures can be found in [10].

These methods allowed for the development of several models to predict the thermal conductivity of two phase or multi-phase systems. One of the first models developed was the Hamilton and Crosser model (Eq. (1)) which has been a starting point for many studies when developing a model for the thermal conductivity of nanofluids. It accounts for the shape of the particles being used and the volume fraction of the discontinuous phase [11].

$$k_r = k_{bf}\left(\frac{k_p+(n-1)k_{bf}-(n-1)\varphi(k_{bf}-k_p)}{k_p+(n-1)k_{bf}+\varphi(k_{bf}-k_p)}\right) \quad (1)$$

where $n = 3/\varphi$ is the shape factor of particles and $\varphi = 3$ for spherical particles. Although this model is frequently used there are a number of limitations, as a shape factor is considered with n, it has to be considered that there may be variations of particle shape within a batch and the orientation may be less random than the equation assumes [11].

Another well-developed model for the calculation of the thermal conductivity is the Maxwell equation [12], Jeffrey emphasised the fact that the Maxwell equation (Eq. (2)) was a first order correction and was not applicable to all volume concentrations [13].

$$k_{Maxwell} = \frac{k_p+2k_{bf}+2(k_p-k_{bf})\varphi}{k_p+2k_{bf}-(k_p-k_{bf})\varphi}k_{bf} \quad (2)$$

Although the Maxwell equation has its limitations as it comes with an assumption that all of the particles are spherical, have a uniform size and there is a low particle concentration leading to no interactions between particles [5]. As it only accounts for the volumetric concentration of the particles and the thermal conductivities of the two phases, it is a simple base model that is easy to use but could lead to a slightly higher error if the particle shape is significantly different [14].

Additional models have also been created to incorporate the particle distribution and the particle/particle interaction within the fluid. Equation 3 shows the model for the thermal conductivity incorporating particle/particle interaction.

$$\frac{k_r}{k_{bf}} = 1 + 3\beta c + c^2\left(3\beta^2 + \frac{3\beta^3}{4} + \frac{9\beta^3}{16}\frac{\alpha+2}{2\alpha+3} + \frac{3\beta^4}{2^6} + \cdots\right) \quad (3)$$

where $\alpha = \frac{k_{nf}}{k_{bf}}$ and $\beta = \frac{k_{nf}-k_{bf}}{k_{nf}+2k_{bf}} = \frac{\alpha-1}{\alpha+2}$ although the series slowly converges and could take over 100 terms to be accurate to 3 significant figures. The equation also assumes that the two particles interacting are spherical in shape and identical in size to allow for symmetry [13].

Various other models have also been developed in an attempt to more accurately predict the thermal properties of a

nanofluid across a wide variety of situations. Angayarkanni and Philip [15] made a comprehensive table of the proposed thermal conductivity models with remarks which is shown in Table 1.

Table 1. *Showing a variety of thermal conductivity models with remarks, reproduced from [15].*

Author(s)	Model	Remarks/Considerations
Maxwell [16]	$\frac{k_r}{k_{bf}}=\frac{1+2\beta\varphi}{1-\beta\varphi}$ where $\beta=\frac{k_p-k_{bf}}{k_p+2k_{bf}}$	Dilute spherical particles/composites
Bruggeman [17]	$\frac{k_r}{k_{bf}}=k_{bf}\frac{(3\varphi-1)\frac{k_p}{k_{bf}}+(2-3\varphi)+\sqrt{\Delta}}{4}$ where $\Delta=(3\varphi-1)^2\left(\frac{k_p}{k_{bf}}\right)^2+(2-3\varphi)^2+2(2+9\varphi-9\varphi^2)\left(\frac{k_p}{k_{bf}}\right)$	Particle Interaction
Hamilton and Crosser [11]	$k_r=k_{bf}\left(\frac{k_p+(n-1)k_{bf}-(n-1)\varphi(k_{bf}-k_p)}{k_p+(n-1)k_{bf}+\varphi(k_{bf}-k_p)}\right)$	Two-component systems of different particles shapes and sizes
Yu et al. [18]	$\frac{k_r}{k_{bf}}=\left(1+\frac{n\varphi A}{1-\varphi A}\right)k_1$ where $A=\frac{1}{3}\sum_{j=a,b,c}\frac{k_{pj}-k_{bf}}{k_{pj}+(n-1)k_{bf}}$	Modified H-C model, particle-liquid interfacial layer consideration
Hashin and Shtrikman [19]	$k_{bf}\left[1+\frac{3\varphi[k_r]}{3k_{bf}+(1-\varphi)k_r}\right]\le k_r\le k_p\left[1-\frac{3(1-\varphi)[k_r]}{3k_p-\varphi[k_r]}\right]$	Series and parallel modes of thermal conduction
Avsec et al. [20]	$\frac{k_r}{k_{bf}}=\left[\frac{k_p+(n-1)k_{bf}-(n-1)\alpha_e(k_{bf}-k_p)}{k_p+(n-1)k_{bf}+\alpha_e(k_{bf}-k_p)}\right]$	Liquid layer thickness
Xuan et al. [21]	$\frac{k_r}{k_{bf}}=\frac{k_p+2k_{bf}+2(k_p-k_{bf})\varphi}{k_p+2k_{bf}-(k_p-k_{bf})\varphi}k_{bf}+\frac{\rho_p\varphi c_p}{2}\sqrt{\frac{k_BT}{3\pi r_c\mu}}$	Brownian motion
Pak and Cho et al. [22]	$\frac{k_r}{k_{bf}}=1+7.47\varphi$	Assumed k enhancement due to suspended particle
Kumar et al. [23]	$\frac{k_r}{k_{bf}}=1+C\frac{2k_BT}{m\mu d_p^2}\frac{\varphi r_{bf}}{k_{bf}(1-\varphi)r_p}$	Brownian motion and temperature
Chandrasekar et al. [24]	$\frac{k_r}{k_{bf}}=\left(\frac{k_p+(n-1)k_{bf}-(n-1)(1+\beta)^3\varphi(k_p-k_{bf})}{k_p+(n-1)k_{bf}-(1+\beta)^3(k_p-k_{bf})}\right)+\frac{C\varphi(T-T_0)}{\mu ka^4}$	Brownian motion and temperature
Prasher et al. [25]	$\frac{k_r}{k_{bf}}=(1+ARe^mPr^{0.333}\varphi)\left[\frac{k_p+2k_{bf}+2(k_p-k_{bf})\varphi}{k_p+2k_{bf}-(k_p-k_{bf})\varphi}\right]k_p$ $h=\frac{k_p}{a(1+ARe^mPr^{0.333}\varphi)}$	Convection caused by Brownian motion
Leong et al. [26]	$\frac{k_r}{k_{bf}}=\frac{(k_p-k_{lr})\varphi k_{lr}[2\gamma_1^3-\gamma^3+1]+(k_p+2k_{lr})\gamma_1^3[\varphi\gamma^3(k_{lr}-k_{bf})+k_{bf}]}{\gamma_1^3(k_p+k_{lr})-(k_{lr}-k_{lr})\varphi[\gamma_1^3+\gamma^3-1]}$	Interfacial layer
Yamada et al. [27]	$\frac{k_r}{k_{bf}}=\frac{\frac{k_p}{k_{bf}}+K-K\varphi\left(1-\frac{k_p}{k_{bf}}\right)}{\frac{k_p}{k_{bf}}+K+\varphi\left(1-\frac{k_p}{k_{bf}}\right)}k_{bf}$ where $K=2\varphi^{0.2}\left(\frac{l_p}{d_p}\right)$	Cylindrical Particles
Gupta et al. [28]	$k_r=k_{bf}(0.0556Pe+0.1649Pe^2-0.0391Pe^3+0.0034Pe^4)$	Effect of translational motion of nanoparticle
Hesselman et al. [29]	$\frac{k_r}{k_{bf}}=\frac{[\alpha(1+2\beta+2)]+2\varphi[\alpha(1-\beta)-1]}{[\alpha(1+2\beta+2)]-\varphi[\alpha(1-\beta)-1]}$	Thermal barrier resistance at interface between materials for spherical, cylindrical and flat plate particles
Xie et al. [30]	$\frac{k_r}{k_{bf}}=1+3\Theta\varphi_T+\frac{3\Theta^2\varphi_T^2}{1-\Theta\varphi_T}$ and $\Theta=\frac{\beta_{lf}[(1+\gamma)^3-\beta_{pl}/\beta_{fl}]}{(1+\gamma)^3+2\beta_{lf}\beta_{pl}}$ where $\beta_{lf}=\frac{k_l-k_f}{k_l+2k_f}$, $\beta_{pl}=\frac{k_p-k_l}{k_p+2k_l}$ and $\beta_{fl}=\frac{k_f-k_l}{k_f+2k_l}$	Effect of nanolayer
Jang et al. [31]	$\frac{k_r}{k_{bf}}=k_{bf}+(1-\varphi)+k_p\varphi+\varphi h_t\delta_T$	Thickness of liquid layer, Brownian motion of dispersed particles
Timofeeva et al. [32]	$\frac{k_r}{k_{bf}}=1+3\varphi$	Agglomeration of Al_2O_3
Wang et al. [33]	$\frac{k_r}{k_{bf}}=\frac{(1-\varphi)+3\varphi\int_0^\infty\frac{k_{cl}(r)n(r)}{k_{cl}(r)+2k_f}dr}{(1-\varphi)+3\varphi\int_0^\infty\frac{k_fn(r)}{k_{cl}(r)+2k_f}dr}$	Effect of clusters
Emami et al. [34]	$\frac{k_r}{k_{bf}}=\frac{\alpha'\left(1+\frac{\Delta}{d}\right)}{1+\frac{\alpha'\Delta}{d}}$ where Δ (m) is the mean free path of nanoparticles.	Thermal resistance
Wang et al. [35]	$\frac{k_r}{k_{bf}}=1+\frac{3fq(p)/p_0}{1-fq(p)/p_0}$	Nanoparticle size, volume fraction shape, nano-layer and interaction between particles
Corcione [36]	$\frac{k_r}{k_{bf}}=1+4.4Re^{0.4}Pr^{0.66}\left(\frac{T}{T_{fr}}\right)^{10}\left(\frac{k_p}{k_{bf}}\right)^{0.03}\varphi^{0.66}$	Considered freezing point
Bu-Xuan Wang et al. [37]	$k_{cp}=k_{ad}\frac{(k_p+2k_{ad})+2A^3(k_p-k_{ad})}{(k_p+2k_{ad})-A^3(k_p-k_{ad})}$ where $A=\frac{1-t}{t+a}$, t (m) is the thickness of the liquid adsorption layer on the surface of the nanoparticles, a (m) is the radius of a particle. k_{cp} (W m^{-1} K^{-1}) is the thermal conductivity of the clustering particles and k_{ad} (W m^{-1} K^{-1}) is the thermal conductivity of	Cluster size and adsorption layer

Author(s)	Model	Remarks/Considerations
	adsorbed liquid layer.	
Chon et al. [38]	$\frac{k_r}{k_{bf}} = 1 + 64.7\varphi^{0.746}\left(\frac{d_f}{d_p}\right)^{0.369}\left(\frac{k_p}{k_{bf}}\right)^{0.7476} Pr^{0.9955} Re^{1.2321}$	Brownian motion and Reynolds number
Kihm et al. [39]	$\frac{k_r}{k_{bf}} = 1 + C\frac{f^a k_b \rho_p c_p T^{1.5}}{k_{bf} h \mu^{0.5} d_p^{0.5}} \exp\left(\frac{-3.8T_b}{T}\right)\left(\frac{c_f}{c_p}\right)^b$ where T_b (K) is the boiling temperature of the base fluid, C, c_f and c_p are emperical constants.	Heat propagation velocity scales
Evans et al. [40]	$\frac{k_r}{k_{bf}} = 1 + 3\varphi\frac{(\gamma - 1)}{\gamma + 2}$	EMT at low volume fraction of well dispersed nanoparticles
Evans et al. [41]	$\frac{k_r}{k_{bf}} = 1 + \varphi\frac{k_p}{3k_1}$	Particle thermal conductivity
Yang et al. [42]	$\frac{k_r}{k_{bf}} = 1 + 3\varphi\frac{\alpha - 1}{\alpha + 2};\ \alpha = \frac{r_p}{R_b k_{bf}}$	Diffusion conduction and Brownian motion
Braginsky et al. [43]	$k_{min}^{-1} = \varphi k_s^{-1} + (1 - \varphi)k_1^{-1}$ $k_{max} = \varphi k_s + (1 - \varphi)k_1$	Correlation function approach and considered particle morphology and agglomeration
Vajjha et al. [44]	$\frac{k_r}{k_{bf}} = \left[\frac{k_p + 2k_{bf} - 2(k_{bf} - k_p)\varphi}{k_p + 2k_{bf} + (k_{bf} - k_p)\varphi}\right] \times 5 \times 10^4 \beta\varphi\rho_{p,bf}\sqrt{\frac{kT}{\rho_p d_p}} f(T, \varphi)$	Particles size range of 27-77 nm
Ho et al. [45]	$\frac{k_r}{k_{bf}} = \frac{2 + \left(\frac{k_p}{k_{bf}}\right) + 2\varphi\left[\left(\frac{k_p}{k_{bf}}\right) - 1\right]}{2 + \left(\frac{k_p}{k_{bf}}\right) - \varphi\left[\left(\frac{k_p}{k_{bf}}\right) - 1\right]}$	For Al_2O_3/water nanofluids

2.2. Convective Heat Transfer

Convective heat transfer has always been an industrial focus due to its effectiveness and high efficiency compared to conduction and radiation [46]. Vegad et al. [47] investigated the effects of nanofluids flowing around a circular cylinder at a low Reynolds number whilst ignoring buoyancy effects, it was found that the Nusselt number increased as the volume fraction of nanoparticles increased. The characteristic equations for mass transfer, momentum and energy equations were solved at steady state and the finite-volume method was used to perform the computations.

A paper was published by Milnea and Lorenzini [48] investigating the effects of a ZnO based nanofluid on natural convection, during this investigation a numerical analysis was performed for the heated wall position, the volume fraction of nanoparticles and the Rayleigh number. An entropy generation analysis was also performed, and it was found that the entropy generation increased as the volume fraction increased, whilst the Nusselt number remained nearly constant. It was also found that if the heat source was from the top, the Nusselt number decreased and entropy increased as the Rayleigh number increased, and the Nusselt number remained constant when the heat source was on the left and the entropy decreased as Rayleigh number increased.

2.3. Boiling Heat Transfer (Pool and Flow Boiling)

Studies to examine the boiling heat transfer effect from nanofluids have been researched in several areas, Okawa et al. [49] investigated the effects of nanoparticle deposition on a hot wall by letting singular drops hit the heated wall at various speeds. A TiO_2/water nanofluid was used and it was found that the deposition of nanoparticles on the surface improved the surface wettability although, if the temperature of the plate was too high, the Leidenfrost effect would hinder the cooling process from the droplets. The main focus was to modify the Weber number above and below the critical velocity to determine the effects of the droplets as they impacted the heater. It was concluded that with a nanoparticle coated surface the vaporisation of the droplet was so rapid that it caused the heat transfer coefficient to decrease but if the temperature was within a suitable range, the CHF could be increased by up to 50% within the confines of the experiment.

Further studies of the boiling heat transfer effects of nanofluids were performed by Lotfi and Shafii [50] with the quenching of a high temperature silver sphere (700 °C) where it was noted that the sphere was quenched faster through nucleate boiling and the overall quenching with nanofluids was reduced compared to that of pure water. It was also found that the cooling time was proportional to the inverse of the nanoparticle concentration. It was proposed that the slower quenching rate was due to the film boiling flux of the nanofluid being lower than that of pure water and because the TiO_2 nanoparticle layer that deposited on the surface acted as an insulator for the sphere.

Vafaei [51] also investigated a similar case to Lotfi and Shafii. The main features examined were the role of the deposited nanoparticles, the effect of the particles on the surface roughness of the heater using SEM, the effect of the nanofluid on the boiling heat transfer coefficient and the surface wettability of the nanofluid. It was concluded that the boiling heat transfer coefficient is not only dependent on the cavity size and the wettability of the nanofluid, but also the range of heat flux as low heat fluxes only activated larger cavities while higher heat fluxes also activated smaller cavities for nucleate boiling. It was also concluded that the deposition of nanoparticles modified the radius of departing bubbles during boiling.

2.4. Currently Known Mechanisms

During experimental investigations of nanofluids, many mechanisms for heat transfer have been hypothesised. Some

of the well reported mechanisms are the increase in thermal conductivity allowing for faster transfer of heat away from the source [52, 53]. The deposition of nanoparticles from which it is proposed that the number of nucleation sites can increase for pool boiling and that capillary wicking can also take place [54-56]. Finally, changes in the surface wettability and contact angle allowing for better liquid contact with the heating surface, further resulting in increased heat transfer were also investigated [54, 57-62].

During the creation of several theoretical models, many further mechanisms of heat transfer enhancement have been proposed, with those from the Brownian motion of the nanoparticles [63-65] although at very low volume concentrations of particles, the enhancement from Brownian motion may be minimal.

3. Critical Heat Flux (CHF)

The CHF is of main concern across various sectors where heat needs to be removed at a significant rate, if the critical heat flux is exceeded, the boiling type changes from nucleate pool boiling to film boiling which results in a significant drop in the heat transfer rate. As the CHF is found to be greatly enhanced by small volume fractions of nanoparticles ($\varphi < 1\%$) with CHF values up to 270% enhancement above that of the base fluid being reported in the literature for homogeneous nanofluids [66] and values up to 480% being reported for hybrid nanofluids [67]. Various models to predict the CHF dependent on certain factors have been developed but the most common way to predict the CHF during pool boiling is the Zuber correlation (Eq. (4)) which incorporates instability as the liquid and vapour compete for the same space between pool and film boiling [68].

$$q_{CHF} = 0.131\rho_v^{0.5}[\sigma g(\rho_l - \rho_v)]^{0.25} \quad (4)$$

where ρ_l (kg m^{-3}) and ρ_v (kg m^{-3}) are the densities of liquid and vapour, respectively. Within the literature, studies concerning the CHF have focused on various mechanisms that could affect the CHF, such as the heating surface orientation and roughness [69]. The effects of the deposited nanoparticle layer on the CHF enhancement [70-72], and the nanofluid stability on the CHF over time [73]. Other articles also examine the effects of the thermos-physical properties and particle concentration effects on the CHF [72, 74, 75].

3.1. Effects of Surface Orientation

When determining the effects of the surface orientation and contact angle on the CHF the Zuber model becomes less accurate, although Kandlikar [76] proposed a model for the estimation of the saturated pool boiling CHF for pure liquids incorporating these factors which is shown in Eq. (5).

$$q_{CHF} = h_{lv}\rho_v^{0.5}\left(\frac{1+cos\theta}{16}\right)\left[\frac{2}{\pi}+\frac{\pi}{4}(1+cos\theta)cos\phi\right]^{1/2} \times [\sigma g(\rho_l - \rho_v)]^{0.25} \quad (5)$$

The effects of the heater orientation was investigated by Dong et al. [77] although the initial investigation was to find whether a relationship between the width of the heater, the material type used and the CHF existed, the results included various inclination angles and showed a general trend that as the inclination angle increased, the CHF also increased. It was proposed that the faster removal of bubbles allowed this further increase in the CHF, Figure 1 depicts the set-up for measuring the CHF showing a cylindrical vessel with vertical copper heaters of varying width used to heat the nanofluid and a glass window to observe the boiling taking place. Figure 2 represents the change in CHF with increasing inclination angle and two different materials.

Figure 1. *A depiction of a set-up for observing the CHF using vertical heating elements of varying width. Adopted from [77].*

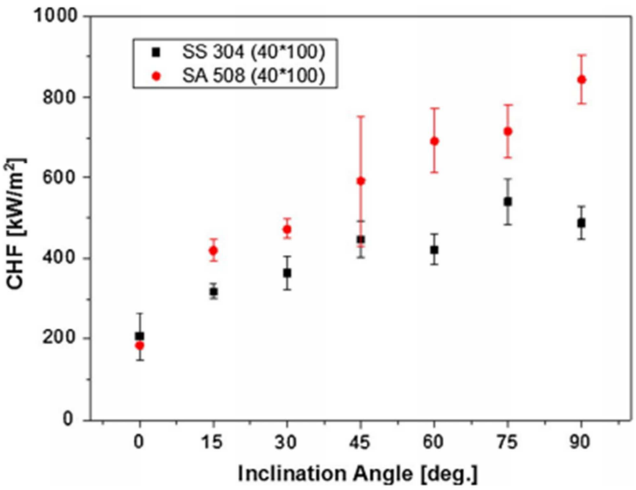

Figure 2. *The change in CHF with increasing inclination angle for a narrow testing section and two different materials. Adopted from [77].*

Another study that investigated the effects of angle was that of Dadjoo et al. [69] where the main focus was the orientation and roughness on the heater surface. Using a SiO_2/water nanofluid of concentration < 0.1 vol% various inclination angles were used between 0° and 90° and it was found to be in agreement with Dong et al, although it was also reported that the boiling heat transfer coefficient decreased as the angle increased. It was proposed that the

increased inclination angle allowed for a greater surface wettability, thus increasing the CHF. It was also stated that the movement of bubbles had an important effect on the nanofluid boiling over the inclined surface.

An alternative model for calculating the CHF with wettability effects was produced in 2012 by Phan et al. [78]. The study included various measurements of micro and macro contact angles and it was stated that the model is in good agreement with existing models on sub-cooled boiling. It was also stated that the model gives a good prediction of the CHF enhancement of 80% of the data in the literature within +/- 30% accuracy.

$$q_{CHF} = \frac{32}{\pi}\frac{K_l K_a}{K_d^3}\left[C_p(T_s - T_\infty) + h_{lv}\right] \quad (6)$$

where $K_l = 0.59\left(\frac{\sigma g(\rho_l - \rho_v)}{\rho_l^2}\right)^{\frac{1}{4}}$; $K_d = \left(6\frac{\sqrt{3}}{2}\right)^{\frac{1}{3}}\left(\frac{\rho_l}{\rho_v}\right)^{-\frac{1}{2}}\left(\frac{\rho_l}{\rho_v} - 1\right)^{\frac{1}{3}} L_c$ in which L_c (m) is the capillary length, $K_a = \pi\rho_l\left[\frac{\sqrt{3}}{2}\left(\frac{\rho_l}{\rho_v}\right)^{-\frac{1}{2}} h_c\right]^3$, C_p (J kg–1 K–1) is the specific heat capacity of the particles, h_{lv} (J kg–1) is the heat of vaporisation. The surface orientation is not the only factor that affects the CHF for nanofluids, various studies have also reported that deposition is a key mechanism for the enhancements seen during experiments.

3.2. Effects of Nanoparticle Deposition

Although the enhancement of heat transfer due to nanoparticle deposition has been reported in a wide range of literature, some further studies have been performed to determine whether there is an optimal concentration of nanoparticles or an optimal nano-layer thickness that would give the largest CHF enhancement. Park et al. [70] used an alumina nanofluid with an average particle diameter of 50 nm and a concentration of 0.01 vol% to determine the effects that the thickness of the nanoparticle deposition had on the contact angle and the CHF of a system. The boiling time of the nanofluid was varied to try to control the quantity of nanoparticles deposited with pre-coating times ranging from 1 minute to 180 minutes. It was found that having shorter pre-coating times and longer heating times had a positive effect on the CHF enhancement with an enhancement of 120% being reported after being heated between four and ten minutes. It was also reported that after longer periods of pre-coating the change in CHF gradually decreased and it was proposed that the deposited layer disturbs the heat flow from the surface.

Ahn and Kim [71] also studied the effects of the deposited nanoparticle layer using an alumina/water nanofluid with a copper upward facing heater. A comparison was made between pure water boiling before nanoparticle deposition, alumna nanofluid being boiled and that of water being boiled after nanoparticle deposition. A high-speed camera was used to observe the CHF phenomenon during the experiment and it was found to be in agreement that the deposition of nanoparticles enhanced the CHF with a CHF of water boiling before deposition being reported as 1532 kW m^{-2} and a value of 1900 kW m^{-2} after nanoparticle deposition. It was also reported that a bend in the boiling curve was observed at higher heat fluxes and that the nanoparticle layer acted similar to a porous medium.

Choi, Kam and Jeong [79] performed an experiment where magnetite nanoparticles were deposited evenly among a vertically arranged testing tube to determine the effects of deposition on the sub-cooled flow boiling CHF. It was found that CHF enhancements between 0 and 40% could be achieved using mass flow rates between 1000 and 5000 kg m^{-2} s^{-1} and sub-cooled inlet temperatures of 40, 60 and 80 °C. The enhancement of the CHF was mainly seen in the high flow rate region of 4000 – 5000 kg m^{-2} s^{-1} whereas even small reductions in the CHF were seen between 1000 and 3000 kg m^{-2} s^{-1}. The explanation of the increased CHF was given to the reduced contact angle on the nano-deposited surface allowing capillary wicking effects to take over as well as having improved wettability.

As nanoparticles are known to deposit on the heater surface creating nano structures, further CHF predicting models have been produced to account for this effect, as well as the capillary wicking effects resulting from the nano-porous structures. A model was produced in 2017 by Li and Huang [80] to account for various micro/nano structures on the heater surface. The formations used were a micro-pillar, micro-ridge structure and random roughness. It was proposed that the CHF enhancement could be accounted for using Kandlikar's model (Eq. (5)) and adding in an extra factor of, "q_{add}". The resulting model is shown in Eqs (7) and (8).

$$q_{add,pillar} = Mh_{lv}h\sqrt{\left(\frac{P-d}{P^2}\right)gcos\theta\rho_l\Delta P} \times \left(\frac{(P-d)d}{sin\alpha P^2}\right) \quad (7)$$

$$q_{add,ridge} = Mh_{lv}h\sqrt{\left(\frac{P-d}{P^2}\right)gcos\theta\rho_l\Delta P} \quad (8)$$

where M is a resultant factor obtained by fitting experimental data. It was also stated that the model has a mean absolute error of 13.7% +/- 25% and although the analyses were based on square pillars, they are applicable to circular pillars.

Ahn et al. [81] also produced a model similar to this accounting for the capillary wicking effects which are seen after deposition, in this model an extra parameter was also added to Kandlikar's equation (Eq. (5)) named, "q''_{gain}" to provide a more accurate prediction of the CHF. This model is shown in Eq. (9).

$$q_{gain} = \left(\frac{\epsilon\delta\rho_f h_{lv}}{A_{heating}}\right) \times \left(\frac{dA_{wetted}}{dt}\right) \quad (9)$$

where δ (m) and $\left(\frac{dA_{wetted}}{dt}\right)$ (m^2 s^{-1}) represent the thickness of the nano/microstructures and the time differential of the wetted area respectively. The result when combined with Kandlikar's equation is represented in Eq. (10).

$$q_{CHF} = Sh_{lv}\rho_v^{0.5}\left(\frac{1+cos\beta}{16}\right)\left[\frac{2}{\pi} + \frac{\pi}{4}(1+cos\beta)cos\phi\right]^{1/2} \times$$

$$[\sigma g(\rho_l - \rho_v)]^{0.25} + \left(\frac{\epsilon\delta\rho_f h_{lv} K}{A_{heating}}\right)\left(\frac{dA_{wetted}}{dt}\right) \quad (10)$$

where K is a fitting factor of 0.55 to fit the experimental results based on the heat flux gain from capillary wicking, it was also stated that the model was in good agreement with experimental data.

Park et al. [82] performed an experiment where CNTs and graphene were spray deposited onto a heater surface. During the experiment, oxidized CNTs and graphene were spray deposited onto the heater surface and it was shown that the heat transfer coefficient linearly decreased with the spray time whilst the CHF increased. From this it was also proposed that a correction factor should be added to Kandlikar's equation (Eq. (5)) to allow for this as shown in Eq. (11).

$$q_{CHF} = C_{cl} h_{lv} \rho_v^{\frac{1}{4}} \frac{1+cos\theta}{16}\left[\frac{2}{\pi} + \frac{\pi}{4}(1+cos\theta)cos\phi\right] \times [\sigma g(\rho_l - \rho_v)]^{\frac{1}{4}} \quad (11)$$

where $C_{cl} = 1.154e^{-0.1sin\theta}$, it was stated that the addition of this correction factor results in a maximum error of 7% to the results of the experiment; it was also stated that there was a good agreement with the data from other researchers.

As nanoparticle deposition is a key mechanism in the enhancement of the CHF, several studies have been performed to determine whether modifying the heater surface in other ways can affect the CHF.

3.3. Heater Surface Modification

In 2015, Mori et al. [83] had performed an experiment to see how the CHF was affected by adding a nanoparticle coating to the heating surface and then adding a porous honeycomb plate in addition to the nanoparticle coating. The results stated that the addition of a porous plate to the heater further increased the CHF, as an expansion to this experiment, in 2017 the effects of adding a honeycomb porous plate and a gridded metal structure to the surface were investigated. An enhancement of up to 3 times that of a plane copper heated surface was reported using a TiO_2/water nanofluid, with gaps of 0.15 μm for the honeycomb layer, it was proposed that the capillary action enhanced the liquid supply and the deposition of nanoparticles increased the wettability and capillary functions on the heater [84].

Mori and Utaka [85] wrote a review that focused on the surface modification effects on the CHF during saturated pool boiling. It was stated that there were several surface modifications possible to enhance the CHF, ranging from adding a porous structure to the heater surface to improve the liquid/vapour flows to the heater, to adding a thin porous coating to the surface to allow for more nucleation sites to be activated. It was concluded that the CHF is enhanced by increasing the surface area on the heater and several recommendations were made for future research including that CHF models that have been proposed need to be validated.

Song and Chang [86] performed experiments using wire nets as a cheaper alternative to using nanoparticle deposition for enhancing the CHF. In this study a forced convection set-up was used with mass fluxes of 1000, 2000 and 4000 kg m^{-2} s^{-1} and pressures of 1.2 and 1.5 MPa. It was reported that CHF enhancements of 103 and 114% were achieved at 1.2 and 1.5 MPa respectively, the explanation of these enhancements were similar to those achieved by nanoparticle deposition. The rapid detachment of bubbles as well as enhanced capillarity and additional nucleation sites led to these enhancements.

3.4. Experiments and Various Other Models

There are several areas of interest when it comes to the applications and functionality of nanofluids as a heat transfer medium, many experiments have been performed on microchannels as a way to assure good performance for electronic cooling and other functions. Vafaei and Wen [87] performed experiments in microchannels and examined correlations found when using nanofluids. It was reported that as the mass flux increased, the CHF also increased although the rate of increase was seen to slow at higher mass flow rates. They also came to agreement that surface modification resulted in a change of the contact angle and increased surface wettability. It was also noted that the enhancement seen to the CHF was dependent on the material type and the length to diameter ratio of the micro-channel, and it was concluded that although enhancements were seen to the CHF, the results were not suitable for larger applications.

Ahn et al. [88] investigated the enhancement of the CHF for forced convective flow boiling of nanofluids with an Al_2O_3/water nanofluid at a volume concentration of 0.01%. Velocities from 1 m s^{-1} to 4 m s^{-1} were used and it was reported that the CHF was enhanced by increasing velocity with increases of 24% at 1 m s^{-1} and 40% at 4 m s^{-1}. The deposition of nanoparticles was also noted with a change in the surface roughness determined by SEM images and that the surface wettability change due to deposition was a key factor in the CHF enhancement.

Mourgues et al. [89] investigated the effects of orientation on the CHF using a ZnO nanofluid of volume concentration 0.01%, the pH was shown to be greater than 8 which was shown to be stable for ZnO nanofluids in their previous work. During the experiment CHF enhancements of up to 54% were observed with a ZnO nanofluid and a nanoparticle deposit, although the CHF for the higher temperatures was not reached. Thus, it was stated that it could be in excess of 100% enhancement. It was proposed that the CHF enhancements were due to the porosity of the deposited layer, capillary wicking as well as the increased roughness and wettability of the surface. Although the primary enhancement was from the deposition of particles rather than the particles in the bulk fluid.

Ahn et al. [90] performed experiments using a reduced graphene oxide (RGO) nanofluid on a silicon dioxide heated surface, the nanofluid was composed of 0.0005 wt% RGO/water. The graphene flakes were characterised using

atomic force microscopy (AFM) and had a thickness of 0.675 nm and a length of 0.5 – 1.0 μm. As graphene is hydrophobic, the deposited layer increased the contact angle of the fluid but also increased the boiling heat transfer by 65% and the CHF by 70%. It was proposed that the enhanced thermal conductivity of the RGO flakes could be the reason for the improved boiling performance and the onset of hot/dry spots being formed could be delayed by this improved heat dissipation. It was stated that the improved heat dissipation could be the reason for the CHF enhancement and due to cavities formed in the deposited layer, the bubble departure frequency was increased.

In 2011, Huang, Lee and Wang [91] performed an experiment investigating the effects of a TiO_2 nanoparticles deposited on a Ni-Cr wire. The deposits were created by submerging a heated wire in TiO_2/water nanofluids of varying concentrations between 0.01 and 1 wt%. The resulting deposits led to an enhancement in the CHF of up to 82.7% when boiling pure water, this enhancement was reached by boiling the wire in a 1 wt% TiO_2 nanofluid with a heat flux of 1000 kW m^{-2}. It was stated that the contact angle with the wire was reduced after deposition occurred and as the deposited layer is both hydrophilic and porous, it led to increased wettability therefore increasing the CHF. It was also stated that the bulk concentration of the nanofluids did not have much effect on the CHF enhancement and could even hinder the enhancement process.

Song et al. [92] investigated the effects of various concentrations of SiC nanofluid on the CHF, the volume concentrations used were 0.0001, 0.001 and 0.01% in atmospheric pressure. Each of the samples contained SiC nanoparticles of diameter 100 nm and was sonicated between one and three hours, the zeta potential was reported to be between -26 and -31 mV, resulting in a relatively stable nanofluid. It was stated that the CHF and volume concentration are not linearly related and a maximum CHF enhancement of 105% was achieved at volume concentration 0.01%. CHF enhancements of 36.2% and 0% were also reported for volume concentrations of 0.0001 and 0.001% respectively. The surface of the heater was also studied and it was shown that deposition played a role in the enhancement of the CHF as this lowered the contact angle therefore increasing the wettability of the surface, allowing for a higher CHF.

Son et al. [93] performed experiments investigating the effect of nanoparticle deposition using chromia nanoparticles on a nichrome wire. The nanoparticles were deposited by boiling a chromia/water nanofluid of 0.01 and 0.1% volume concentration around a nichrome wire. To change the quantity of nanoparticles deposited the boiling time was changed. It was stated that before the saturated deposition condition was reached, the CHF enhancement achieved increases proportionally to the boiling time of the nanofluid. However, it was also stated that after the deposited layer becomes saturated, further boiling could lower this enhancement. After optimal deposition it was reported that a CHF enhancement of 88.8% was seen with the hydrophilic surface of chromia used to explain the CHF enhancement. Alongside the pool boiling experiments, sputtering experiments of chromia were also performed which gave a maximum CHF enhancement of 93.8%, it was stated that the increased wettability would not be able to explain the sputtering case as it is a non-porous surface.

Lee et al. [94] used laser ablation to produce a CuO nanofluid by a one-step process and also performed experiments using a two-step process to compare the deposition characteristics. A CuO/water nanofluid of volume concentratrion 0.001% was produced by a one-step and a two-step process, the average particle diameters were 15 nm and 55 nm respectively. The zeta potentials of each nanofluid were reported to be 39 mV and 15.8 mV meaning that the nanofluid produced by the one-step process is classed as a stable nanofluid whilst the two-step matter would not be. During the experiment, it was found that the nanofluid produced by the one-step process gave a lower contact angle and a higher CHF enhancement than the two-step process. The contact angle from the one-step production was reduced from 75° to 30° achieving a CHF enhancement of approximately 2.6 times, whilst the two-step nanofluid reduced the contact angle to 61° with an enhancement of approximately 2.3 times that of deionised water. As the focus was the deposition structures of the two different methods, the capillarity was also investigated, it was found that the nanofluid produced by the one-step method also increased the capillarity more than that of the two-step method, resulting in a higher CHF enhancement.

In 2018, Filho et al. [95] performed experiments observing the wettability of surfaces covered with nanoparticles. During the experiments two Al_2O_3 nanofluids of particle diameters 20 – 30 nm and 40 – 80 nm were used as well as two SiO_2 nanofluid of particle diameters 15 nm and 80 nm, the nanofluids were prepared to volume concentrations 0.01, 0.1 and 0.5%. As no stabilising agents were used the stability was approximately one hour. It was found that through nanoparticle deposition, porous nanostructures were created which then changed the spreading mechanism of the liquid from inertial to capillary driven within 10 ms. It was also stated that no relationship between the roughness of the surface and the wettability could be found and that, clusters of nanoparticles play an important role of forming porous chains which contributes to super wetting of a surface.

Further studies have been performed to determine the effects of nanoparticle deposition on heated surfaces. Kim et al. [96] performed experiments using a TiO_2 nanofluid of volume concentration 0.01% produced via a two-step method. The average particle diameter was reported to be 47 nm and the nanofluid was sonicated for three hours. During the experiments the contact angle, capillarity and thickness of the deposited layer were measured, it was reported that a maximum CHF enhancement of approximately 175% was achieved. It was also shown that the CHF generally increased as the thickness of the deposited layer increased as well as higher capillarity. It was concluded that the wettability fails to show CHF enhancement when nanoparticles are deposited

on a thin wire but the capillarity improves the CHF due to the pores holding the liquid macrolayer, increasing the liquid supply and reducing the number of hot/dry spots.

Park et al. [97] investigated the effects of an Al_2O_3/R-123 ($CHCl_2CF_3$) nanofluid with and without a micro-capsulated phase change material (MPCM, $C_{19}H_{40}$) on the CHF. The average dimension of the MPCM was 20 μm (10 – 30 μm). It was stated that the addition of a PCM (phase change material) can result in more nucleate spots for bubbles to form allowing heat to be absorbed away from the surface of the heating source. PCMs can also help to prematurely merge bubbles and bring them away from the heated surface which can prevent the build-up of dry spots, delaying the onset of the CHF. During the experiment, nanofluids of volume concentrations 0.001% – 1% were created and sonicated for five hours, a table of various CHF enhancements achieved during the experiments was created with varying conditions and is depicted in Table 2.

Table 2. *The CHF enhancement of MPCMs and Al_2O_3 nanoparticles in various conditions. Adopted from [97].*

Case	Dispersed materials in R-123	MPCM pre-coating on the heater	Concentration (vol%)	CHF enhancement ratio (CHF/CHF R-123)
1	No	No	0	1
2	MPCM	No	0.01	1.44
3	No	Yes	0.01	1.24
4	MPCM	Yes	0.01	1.41
5	Al_2O_3	No	0.01	1.71
6	Al_2O_3 + MPCM	No	0.01	1.94
7	MPCM	No	0.001	1.28
8	MPCM	No	0.1	2.12
9	MPCM	No	1	2.24

As carbon nanotubes are of interest for nanofluids various experiments have been performed to see the enhancements that can be obtained by dispersing them throughout a base fluid. Seo et al. [98] performed experiments to determine the effects of a layer by layer assembled deposit on the pool boiling CHF by using a PEI (polyethyenimine)/MWCNT nanofluid. The particle diameters of the CNTs were between 20 and 40 nm with a cluster length of 5 – 20 μm. Atomic force microscopy and SEM were used to determine the characteristics of the deposited bilayers on the surface. Layer thicknesses of 10, 20 and 40 bilayers were deposited on the surface and the CHF tested in each case. It was found that the CHF enhancement increased proportionally to the number of bilayers deposited with a maximum CHF enhancement of 94% being achieved. A pore size of approximately 20 nm gave the highest CHF which implies that not only does the random orientation of the porous network enhance the CHF but also the pore size of the deposited layer. It was stated that the deposition of CNTs on the surface creates a randomly oriented porous structure which led to a wettability increase of approximately 70% as the layer number increased. It was concluded that improving rewetting ability of the porous layer can improve the CHF, the CHF measured was much higher than was predicted by correlations and that no single surface parameter can explain the CHF enhancement in nanofluids.

In 2018, Hu et al. [99] used SiO_2 nanofluids of volume concentrations 0.081, 0.163 and 0.325% with an average particle diameter of 98 nm made by the Stober process (see [100]). Each of the samples was sonicated for 30 minutes and X-ray diffraction was used to determine the components of the nanofluid. A SiO_2 nanofluid was also prepared by a two-step processing method to determine the differences of nanofluids prepared via a wet method (sol-gel processing) and a dry method (two-step processing), it was concluded that the nanoparticles prepared via a wet method were better. This was because when the dry nanoparticles are dispersed throughout a base fluid, a higher amount of aggregate formed. It was found that during the experiments the wettability of the fluid was improved with the lowest volume concentrations of 0.081% giving the highest CHF enhancement of 68.8%. During the experiments, the effect of the mass fraction was observed, and it was found that as the volume concentration increases, the contact angle also increases but the surface tension decreased. Although, the deposition of nanoparticles led to an improvement in the surface wettability which resulted in an increase of the CHF.

Pham et al. [101] performed experiments using both homogeneous and hybrid nanofluids consisting of Al_2O_3, CNTs and a mixture of both. The volume concentrations used were 0.05% in each case with 0.05% of both Al_2O_3 and CNTs being used for the hybrid nanofluid. Each of the samples was sonicated for one hour and boric acid was used to change the pH, after three days, the zeta potentials of the samples were 39 mV, 35 mV and 53 mV for the Al_2O_3, CNT and hybrid nanofluids respectively. The CHF enhancements achieved were 33%, 108% and 122% for Al_2O_3, CNT + boric acid 10% and the hybrid nanofluid respectively. It was reported that the CHF enhancement increased as the incline angle of the heater increased from a downward-facing position to a vertical position although contradictory to this, the maximum CHF enhancements observed were in the downward facing position. It was concluded that the CHF enhancement was not caused by the nanoparticles in the suspension but by the surface modification of the heater, roughness and volume concentration. These factors led to the surface becoming rougher and more hydrophilic, allowing for better liquid contact which results in a higher CHF value.

As most of the literature has a focus on the static CHF, some studies were performed investigating the transient CHF. One such study was by Sharma et al. [102] in 2013. In this experiment a ZnO/water nanofluid was used with a volume concentration of 0.01%, an average particle diameter of 38 – 68 nm and a pH of 8.66 which is in the 8 – 10 range known

to be stable for ZnO suspensions. To measure the effects of the nanofluid on the transient CHF heating time intervals of 1, 10 and 100 s were chosen. The experiment was carried out with both a clean surface and a deposited surface to determine the effects of the deposited nanoparticles on the CHF. It was determined that the transient CHF was higher than the steady state CHF and that the CHF increased with decreasing time interval. Deposition of nanoparticles was seen after 10 s, which led to the formation of a porous and hydrophilic layer on the heater surface. It was also found that the precoated heater showed improvements to the transient CHF in all time intervals while the bare heater only showed significant improvements in the 10 and 100 s intervals. It was then concluded that the enhancement of the CHF was provided by the deposited nanoparticles rather than the particles in the fluid.

Park and Bang [103] performed experiments in order to try and create a universal CHF enhancement mechanism for nanofluids using the hydrodynamic instability of the fluid. During these experiments six different nanofluids, ZnO, SiO_2, SiC, Al_2O_3, GO and CuO were used at volume concentrations of 0.01%. The particle diameters were given as 40 – 100 nm, < 30 nm, < 100 nm, < 50 nm, < 45 nm and between 25 – 37 nm for ZnO, SiO_2, SiC, Al_2O_3, GO and CuO respectively. Overall the preparation of the nanofluids took two hours including sonication for improved stability. It was reported that CHF enhancements between 90 – 160% were achieved with the highest being given by the CuO nanofluid and the lowest being given by the ZnO nanofluid. As the goal was to create a universal mechanism for the CHF enhancement, a model was proposed using the hydrodynamic instability wavelength (Rayleigh-Taylor wavelength) and is shown in Eq. (12).

$$q_{CHF} = 0.52\epsilon^{2.28} h_{lv} \left[\frac{\sigma \rho_l \rho_v}{(\rho_l+\rho_v) r_{po}}\right] \tag{12}$$

where r_{po} (m) is the radius of the pores. This equation was then simplified to Eq. (13).

$$q_{CHF} = q_z \frac{\sqrt{\lambda_{bare}}}{\sqrt{\lambda_{porous}}} \tag{13}$$

where q_z (W m^{-2}) is the heat flux based on the model by Zuber et al [68]. λ (m) is the Rayleigh-Taylor wavelength for the heater. Various heater shapes and dimensions were also given and shown in Eqs (14) – (17) with two versions for 1-D cylindrical heaters experimented.

$$\lambda_{d1,flat} = \frac{2\pi\sqrt{3}}{\sqrt{\frac{g(\rho_l-\rho_v)}{\sigma}}} \tag{14}$$

$$\lambda_{d2,flat} = \sqrt{2}\lambda_{d1,flat} \tag{15}$$

$$\lambda_{d1,cylinder} = \frac{2\pi\sqrt{3}}{\sqrt{\frac{g(\rho_l-\rho_v)}{\sigma}+\frac{2}{D_h^2}}} \tag{16}$$

$$\lambda_{d1,cylinder} = \frac{2\pi\sqrt{3}}{\sqrt{\frac{g(\rho_l-\rho_v)}{\sigma}+\frac{4}{D_h(D_h+2a)}}} \tag{17}$$

where D_h(m) is the diameter of the cylindrical heater. Park et al. [104] performed an experiment using very low concentrations (0.0005 vol%) of graphite nanoplatelets (xGnPs) as a cheaper alternative for carbon nanotubes, an oxidated version of the nanoparticles was also used during the experiments. The platelets were created by the Hummers and Offeman method [105] and dispersed via sonication with zeta potentials of -53.5 mV and -62.5 mV for the xGnPs and the xGnP Oxide platelets respectively, meaning the suspensions are very stable. It was reported that there was no change to the surface morphology of the heating wire used via FE-SEM scans and there was no reduction in the contact angle. The highest CHF enhancement of 189% was reported from the xGnP Oxide nanofluids at a volume concentration of 0.005%, a comparison of the measured CHF was made to the prediction from Kandlikar's equation (Eq. (5)), which was found to be in disagreement. The deviation from that of the predicted CHF was hypothesised to be partially due to capillary wicking from nanoparticle deposition.

Table 3 shows a summary of the results from various experiments for calculating the CHF enhancement with various nanofluids with notes on the experimental conditions and other important factors.

Table 3. *A summary of CHF enhancement values from various literature sources.*

Author(s)	Nanofluid	Vol Conc (%)	Maximum CHF Enhancement (%)	Notes
Neto et al. [72]	Alumina/water, Maghemite/water, CNT/water	0.02 – 0.1	26 – 37	CHF enhancements achieved due to increased wettability of the heating surface rather than the enhanced heat conduction by the addition of nanoparticles
Vazquez and Kumar [66]	SiO_2/water	< 0.5%	250 – 300	Peak enhancement found between 0.2 – 0.4% volume concentration and CHF enhancement declined as volume concentration increased due to increased deposition
Forrest et al. [61]	-	-	44 – 101	Surface of the heating element modified with Si nanoparticles
Park, Bang and Park [106]	Ag/water, Cu/water, Al_2O_3/water	0.001	58, 99, 187	Nanoparticles were created via the electrical explosion of a wire in a liquid
Park et al. [104]	Graphite Nanoplatelets/water, GnP	0.001, 0.005	50, 189	Volume concentrations of 0.001 – 0.03% for GnPs and 0.005 – 0.05% for GnP Oxide, GnP Oxide performed better than Graphite nanoplatelets for CHF enhancement in all cases

Author(s)	Nanofluid	Vol Conc (%)	Maximum CHF Enhancement (%)	Notes
Kim et al. [67]	AL_2O_3/water, RGO (Reduced Graphene Oxide)/water	0.0001 – 0.01 Al_2O_3, 0.00005 – 0.005 RGO	54% at 0.01% vol Al_2O_3, 473	473% enhancement achieved with equal mix of both nanoparticles at vol concentration of 0.0005% each
Vafaei and Wen [87]	Alumina/water	0.001 – 0.1	4 – 31	Study on micro-channels and CHF enhancement by increasing flow rate of nanofluid.
Park, Moon and Bang [70]	Alumina/water	0.01	120	Study on thickness of deposited nanoparticles, maximum CHF enhancement seen after 4 – 10 minutes of heating
Lee et al. [107]	Graphene Oxide/water	0.01	100	Flow boiling experiment with nanofluids with maximum CHF enhancement found at 250 kg m^{-2} s^{-1} and 25 ºC inlet temperature
Dewitt et al. [108]	Al_2O_3/water	0.001 – 0.01	Avg 70, 17 – 108	Flow boiling CHF measured, 30 minutes of boiling time gives substantial CHF enhancement. Lowered contact angle gave higher CHF, CHF relative enhancement not dependent on orientation angle when flow is above 1000 kg m^{-2} s^{-1}. Increasing the concentration by factor of 10 (to 0.01%) provided no extra CHF benefit.
Ahn et al. [109]	RGO/water	0.0005 wt%	320	CHF increases with increased coating time. Water absorbed by the carboxyl group allowing for better liquid contact to enhance CHF. Performed surface analysis, checked deposition, thermal activity, water absorption and Rayleigh-Taylor wavelength.
Cheedarala et al. [110]	CuO-Chitosan/water, CuO/water	0.003, 0.006, 0.03, 0.06 wt%	79	High wettability and nanoporous structure formed on Ni-Cr wire. Contact angle significantly reduced from 72 degrees to 42 degrees at 0.06 wt%. Capillary wicking and an effect of Taylor's modified wavelength used as explanations for CHF enhancement.
Lee et al. [111]	Magnetite (Fe_3O_4) /water, Al_2O_3/water, TiO_2/water	0.0001, 0.01	170 – 240	Diameter of particles 30 +/- 5 nm, sonicated for 3 hours to improve stability, zeta potential measured after 1, 12 and 24 hours. Above 30 mV for all measurement (approx. 31 mV after 24 hr). Surface wettability and surface tension changed, onset of CHF delayed due to lower hot spots (higher bubble frequency). Speculated that magnetic fields can improve CHF via control of local concentration of magnetic nanofluids.
Park and Bang [112]	GO (Graphene Oxide)/water	0.0001	20	GO/water nanofluid with varying mass flow rates. Highest CHF enhancement seen at 50 and 100 kg m^{-2} s^{-1}. Wettability of the surface was not improved therefore the thermal activity of the GO deposited layer is presumed to be the reason for CHF enhancement.
Kim et al. [113]	Al_2O_3/water	0.0001, 0.001	80	Experiment to compare the enhancements of a nanofluid and a nano-deposited tube. Determined that deposition is the main reason for CHF enhancement as the deposited tube and nanofluid CHF results were similar. CHF increases as mass flow rate increases between 500 – 1500 kg m^{-2} s^{-1}, no trend seen between 100 – 300 kg m^{-2} s^{-1}. Concentration has no effect on the CHF enhancement.
Lee et al. [114]	Magnetite (Fe_3O_4)/water	1, 10 and 100 ppm	Approx. 47 without magnetic field, 62 with magnetic field	It was reported that deposition of the nanoparticle had taken place which improved the wettability and re-wetting characteristics. The nanofluid had a particle diameter of 25 nm, was sonicated for three hours and had a zeta potential of 32.61 mV after four days. It was determined that as the thickness of the deposited layer increased, the CHF increased up to a saturated value. Magnetic nanofluids can be controlled via magnetic fields and can be easily removed from the fluid.
Neto et al. [115]	Al_2O_3/water, Maghemite/water, CNTs/water	0.02 – 0.10	26 – 37	Varying particle diameters with Al_2O_3, magnetite and CNTs being 80 – 100 nm, 70 – 100 nm and 50 – 100 nm (apparent d_p) respectively. Static contact angle was stated to be lowered from 85° to 0° showing complete wetting. Deposited layer created a porous outer layer which was responsible for the complete wetting.
Kamatchi and Kumaresan [116]	RGO/water	0.01, 0.05, 0.1, 0.2, 0.3 g L^{-1}	245	No sediment seen after seven days with a zeta potential of -39.1 mV on the fifth day. An increased bubble density with smaller bubbles as well as a porous structure that helped to reduce the wall superheat led to the enhanced CHF.
Kole and Dey [117]	ZnO/EG	0.35 – 3.75	117	Highest CHF enhancement seen at volume concentration of 2.6%. The nanofluid underwent very long periods of sonication (760 hours) with a particle diameter of 30 – 40 nm. After sonicating 12 – 60 hours the average agglomerate size reduced from 419 – 120 nm. A total of 730 days passed with no visible sediment. The CHF is enhanced by the surface roughness increasing via deposition. High concentrations led to sedimentation blocking active nucleate sites which resulted in a lower boiling heat transfer coefficient.

Author(s)	Nanofluid	Vol Conc (%)	Maximum CHF Enhancement (%)	Notes
Park et al. [118]	CNT/water	0.0001, 0.001, 0.01 and 0.05	200	Particle diameter of 10 – 20 nm with a cluster length of 10 – 50 μm. The dispersion was well maintained after 15 days. Maximum CHF enhancement seen at 0.001 vol%. Deposition creates a layer which reduces the contact angle and alters the bubble departure rate. The delayed onset of a vapour canopy formation led to increased CHF.
Kim et al. [119]	GO/water	1, 5, 10 mg L^{-1}	139	Work was compared to previous work on RGO, GO gave a higher CHF enhancement than RGO. No improved wettability was seen but it was stated that the GO layer acted as a heat spreader reducing hot or dry spots. Maximum CHF enhancement was seen at 5 mg L^{-1} which was higher than RGO at 5 mg L^{-1} which gave 80% CHF enhancement.
Kwark et al. [120]	Al_2O_3, CuO, Diamond/water	2.7 x 10^{-5} – 0.001	Approx. 80	At a volume concentration of 0.0007% the BHT is not deteriorated whilst the CHF is increased meaning this concentration is more optimal. Methods for nanoparticle deposition are given as natural nano-particle precipitation, natural convection at low heat flux, applied electrics fields and nucleate boiling. A maximum CHF of approximately 80% was achieved with all of the nanofluids and results were compared to a low system pressure situation resulting in the conclusion that it seems CHF enhancement potential is reduced with increasing system pressure.
Park et al. [121]	GO/water	0.0001	200	The study investigated the affected of using GO/water nanofluid as a nuclear coolant. It tested the effects of the heater orientation angle and the stability of GO nanofluids with boric acid, LiOH and tri-sodium-phosphate (TSP). It was found that GO nanofluids are very stable in a nuclear coolant environment. A maximum CHF enhancement of 200% was found using a horizontal plate, with the CHF enhancement at a heater orientation of 90 degrees being 40%. The possible enhancement for vertical orientation was explained using bubble dynamics, bubbles coalesce and are removed early reducing the dry spots but further up the heat source is vapour blanketed as the bubble rises.
Ahn et al. [122]	RGO/water	0.0001, 0.0005, 0.001 wt%	200	Various layers of RGO were seen deposited on the surface of the heater. It was determined that although RGO shows a hydrophobic nature, there are three layers that are encompass the porous deposited structure. A base graphene layer which is presumed to be hydrophilic resulting in a lower contact angle, a self-assembled foam-like structure and thickly aggregated graphene layer which are determined to be hydrophobic. The maximum enhancement was achieved with a concentration of 0.0001 wt%. It was also concluded that the increased thermal activity of RGO could act as a heat dispersant and reduce hot spots on the surface, therefore delaying the onset of the CHF.
Amiri et al. [123]	CNT/water	0.01, 0.05, 0.1 wt%	289.1	During the experiment the synthesis method of CNTs was tested to determine whether it would affect the CHF enhancement. Three types of CNTs were produced, a normal CNT/water nanofluid, CNT-cystine compound and then a CNT-Ag compound, each of which was then dispersed throughout water. The maximum CHF enhancement was foud using a CNT-cystine/water nanofluid at a concentration of 0.05 wt% which led to the conclusion that the synthesis method of the CNTs can affect the CHF enhancement obtained.
Jung et al. [124]	Al_2O_3/water	0.00001 – 0.1	103	The experiment was to determine the effects of stabilizing agents on the CHF and BHTC of nanofluids. Polyvinyl alcohol (PVA) was used as the stabilizing agent. The maximum CHF enhancement was achieved using a concentration of 0.001 vol%. It was concluded that with the stabilizing agent the CHF slightly increased but the increase was rather insignificant.
Kim et al. [125]	Al_2O_3/water, zirconia/water, SiO_2/water	0.001, 0.01, 0.1	Approx. 80	The main focus of this experiment was to determine the surface wettability change and the effects this had on the CHF. It was shown that there was a porous layer formation on the heater surface by deposition which led to a reduced static contact angle, therefore increasing the CHF. It was hypothesised that the CHF could be due to a multitude of factors such as: hydrodynamic instability, microlayer dryout, hot/dry spot reduction and bubble interaction.

A summary of CHF and heat transfer enhancements from various experiments between 2003 – 2016 can be found in a review written by Fang et al. [75].

Wang et al. [126] performed an experiment investigating the effects of nanofluids on the flow boiling CHF, the experiment was conducted using alumina/water and AlN/water nanofluids with two volume concentrations of 0.1 and 0.5%. The effects of the outlet pressure, sub-cooled inlet temperature, heater length, diameter of the heater, nanoparticle type and concentration were investigated. It was found that the CHF increased as the outlet pressure, mass flux and diameter increased, and it decreased with increasing

heater length with a maximum enhancement of 18% being recorded. It was found that the sub-cooled inlet temperature, nanoparticle type and concentration have no significant effect on the CHF. This experiment led to the development of a correlation to predict the flow boiling CHF which is shown in Eq. (18).

$$q_{CHF} = \Delta T_{sub} C_p G \frac{D_{in}}{4L} + 0.7073 G h_{lv} \left(\frac{D_{in}}{L}\right)^{0.9708} \times \left(\frac{\rho_v}{\rho_l}\right)^{0.2013} \left(\frac{(\rho_l - \rho_v)^{0.5} {u_l}^2}{g^{0.5}\sigma^{0.5}}\right)^{-0.1135} \quad (18)$$

where G (kg m^{-2} s^{-1}) is the mass flux of the nanofluid, D_{in} (m) is the inner diameter of the heat transfer tube. It was stated that this correlation is accurate for a heater diameter of 6 – 8 mm, length of 500 – 800 mm, sub-cooled temperature of 13.5 – 35.9°C, outlet pressure of 0.4 – 0.89 MPa and a mass flux of 98.9 – 349.4 kg m^{-2} s^{-1} [126].

In addition to the models previously mentioned within this section, Liang and Mudawar [127] produced a table showing all of the current models and correlations for predicting the CHF during pool boiling and organised them into groups that take into account orientation effects, as well as orientation effects and the contact angle with remarks for each model. This is given in Table 4.

Table 4. *A table produced by Liang and Mudawar showing a summary of the current models and correlations for predicting the CHF during pool boiling. Adopted from [127].*

Author(s)	Relation(s)
Zuber et al. [68]	$q_{CHF} = 0.131\rho_v h_{lv}[\sigma g(\rho_l - \rho_v)/\rho_v^2]^{1/4}$
Kutateladze [128]	$q_{CHF} = 0.16\rho_v h_{lv}[\sigma g(\rho_l - \rho_v)/\rho_v^2]^{1/4}$
Lienhard & Dhir [129]	$q_{CHF} = 0.149\rho_v h_{lv}[\sigma g(\rho_l - \rho_v)/\rho_g^2]^{1/4}$
Wang et al. [130]	$q_{CHF} = [0.18 - 0.14(P/P_c)^{5.68}]\rho_v h_{lv}[\sigma g(\rho_l - \rho_v)/\rho_v^2]^{1/4}$
Rohsenow & Griffith [131]	$q_{CHF} = 0.012\rho_v h_{lv}[(\rho_l - \rho_v)/\rho_v]^{0.6}$
Haramura & Katto [132]	$q_{CHF} = 0.721\left(\frac{A_v}{A_w}\right)^{5/8}\left(1 - \frac{A_g}{A_w}\right)^{5/16}\left[\left(\frac{\rho_l}{\rho_v} + 1\right)/\left(\frac{11\rho_l}{16\rho_v} + 1\right)^{0.6}\right]^{5/16} \times \rho_v h_{lv}[\sigma g(\rho_l - \rho_v)/\rho_v^2]^{1/4}$ where $\frac{A_v}{A_w} = 0.0584\left(\frac{\rho_v}{\rho_l}\right)^{1/5}$
Yagov [133]	$q_{CHF,l} = 0.5\frac{h_{lv}^{81/55}\sigma^{9/11}\rho_v^{13/110}k_l^{7/110}g^{21/55}f(Pr_l)}{v_l^{1/2}c_{pl}^{3/10}R_l^{79/110}T_{sat}^{21/22}}$ for $\frac{P}{P_c} < 0.001$ where $f(Pr_l) = \left(\frac{Pr_l^{9/8}}{1+2Pr_l^{1/4}+0.6Pr_l^{19/24}}\right)$ $q_{CHF,h} = 0.06h_{lv}\rho_v^{3/5}\sigma^{2/5}[g(\rho_l - \rho_v)/\mu_f]^{1/5}$ for $P/P_c < 0.003$ $q_{CHF} = \left(q''^3_{CHF,h} + q''^3_{CHF,l}\right)^{1/3}$ for $0.001 < P/P_c < 0.003$
Guan et al. [134]	$q_{CHF} = 0.2445\left(1 + \frac{\rho_v}{\rho_l}\right)^{1/4}\left(\frac{\rho_v}{\rho_l}\right)^{1/10}\rho_v h_{lv}[\sigma g(\rho_l - \rho_v)/\rho_v^2]^{1/4}$
Mudawar et al. [135]	$q_{CHF} = 0.151\rho_v h_{lv}[\sigma g(\rho_l - \rho_v)/\rho_v^2]^{1/4}$
El-Genk & Bostanci [136]	$q_{CHF} = [(0.229 - 4.27\times10^{-4}\theta)^{-6} + (0.577 - 2.98\times10^{-3}\theta)^{-6}]^{-1/6} \times \rho_v h_{lv}[\sigma g(\rho_l - \rho_v)/\rho_v^2]^{1/4}$
Vishnev [137]	$q_{CHF} = 0.0125(190 - \theta)^{1/2}\rho_v h_{lv}[\sigma g(\rho_l - \rho_v)/\rho_v^2]^{1/4}$
Arik & Bar-Cohen [138]	$q_{CHF} = 0.131(1 - 0.001117\theta + 7.79401\times10^{-6}\theta^2 - 1.37678\times10^{-7}\theta^3) \times \rho_v h_{lv}[\sigma g(\rho_l - \rho_v)/\rho_v^2]^{1/4}$
Brusstar & Merte [139]	$q_{CHF} = \frac{\pi}{24}\lvert sin\,\theta\rvert^{1/2}\rho_v h_{lv}[\sigma g(\rho_l - \rho_v)/\rho_v^2]^{1/4}$
Chang & You [140]	$\frac{q_{CHF}}{q_{CHF,max}} = 1 - 0.0012\theta\,tan(0.414\theta) - 0.122\,sin(0.318\theta)$
Kirchenko & Chernyakov [141]	$q_{CHF} = 0.171\frac{(1 + 0.324\times10^{-3}\alpha^2)^{1/4}}{(0.018\alpha)^{1/2}}\rho_v h_{lv}[\sigma g(\rho_l - \rho_v)/\rho_v^2]^{1/4}$
Theofanous & Dinh [142]	$q_{CHF} = k^{-1/2}\rho_v h_{lv}[\sigma g(\rho_l - \rho_v)/\rho_v^2]^{1/4}$ where $k = \left(1 - \frac{sin\,\theta}{2} - \frac{\pi/2-\theta}{2\,cos\,\theta}\right)^{-1/2}$
Kandlikar [76]	$q_{CHF} = \frac{1 + cos\,\theta}{16}\left[\frac{2}{\pi} + \frac{\pi}{4}(1 + cos\,\theta)\,cos\,\phi\right]^{1/2}\rho_v h_{lv}[\sigma g(\rho_l - \rho_v)/\rho_v^2]^{1/4}$
Liao et al. [143]	$q_{CHF} = 0.131\left[-0.73 + \frac{1.73}{1 + 10^{-0.021\times(185.4A-\theta)}}\right]\left[1 + \frac{55 - \alpha}{100}(0.56 - 0.0013\theta)\right]\rho_v h_{lv}[\sigma g(\rho_l - \rho_v)/\rho_v^2]^{1/4}$

When it comes to measuring the CHF, it is required to be aware of the equipment previously used in experiments to allow for comparability, the next section briefly discusses the two main types of setups used to measure and visualise the CHF.

3.5. Experiment Setups

When visualising and monitoring the CHF, various setups have been used during the experiments, some setups involve a horizontal electrical wire submerged within a nanofluid. Others prefer to use a flat plate with thermocouples to visualise the pool boiling and CHF from that perspective. Aznam et al. [84] used the setup shown in Figure 3 to visualise both the pool boiling and CHF. The setup consists of a flat-plate copper heater at the bottom of a glass cylindrical vessel to initiate pool boiling and a high-speed camera installed to allow visualisation of the bubbles forming and the CHF in action. Several thermocouples were also used to monitor the temperature of the heat block and a cooling coil with a condenser to cool the gases and allow for a saturated pool boiling environment.

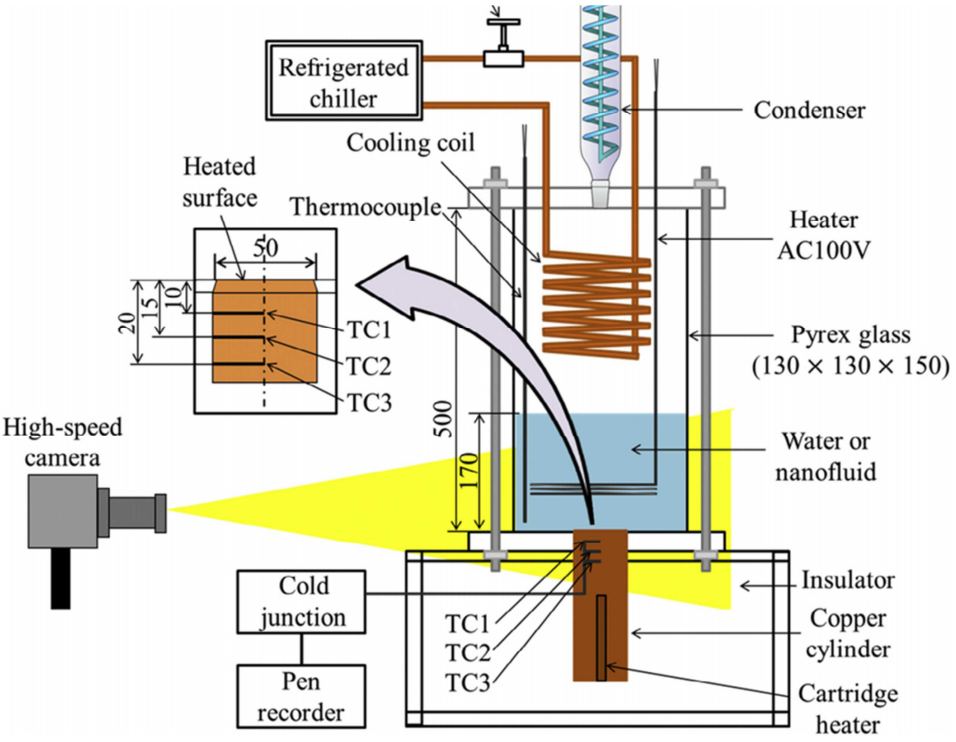

Figure 3. *A diagram representation of the setup used by Aznam et al. to observe the CHF and pool boiling of a nanofluid. Adopted from [84].*

Whilst Aznam et al. used a flat heating surface for their heating source, Park et al. [106] chose to use a horizontal thin wire depicted in Figure 4 to observe the CHF of Ag, Cu and Al_2O_3/water nanofluids. The method chosen by Park et al. gives a better representation of pool boiling around a cylindrical object. The figure depicts a thin NiCr wire attached to two copper electrodes, the wire was submerged in a nanofluid pool which was situated in a glass vessel on top of a heated plate. Current was then passed through the wire to initiate pool boiling of the nanofluid, the temperature of the nanofluid was monitored using a thermo-sensor and a reflux condenser also attached to the top of the vessel to allow for saturated conditions.

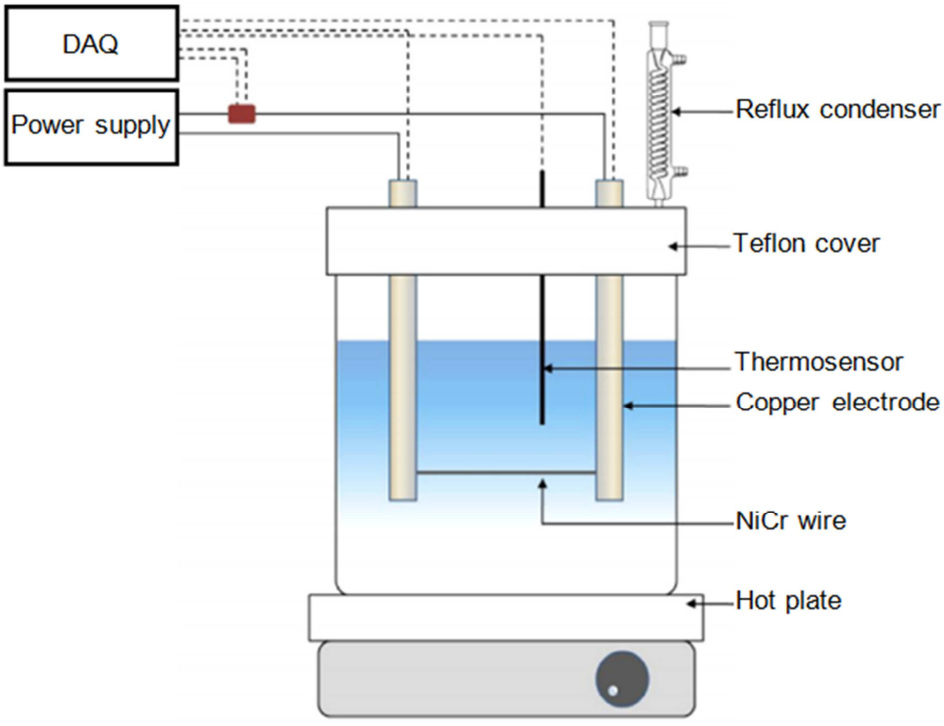

Figure 4. *A depiction of the setup used by Park et al. to observe the pool boiling and CHF of various nanofluids. Adopted from [106].*

Another key feature to be observed after the CHF is the stability of nanofluids, as of yet there is limited research into the use of nanofluids in the extreme regions such as boiling of nanofluids which will be essential for nanofluids to be used in industry.

4. Stability

For the engineering applications of nanofluids, one main concern is maintaining the stability of the nanofluid, allowing for application across a wide range of engineering sectors. Long-term stability can be difficult to attain due to the requirement of long experiments (allowing for the approximation of nanofluid life) and ensuring that the enhanced properties of the nanofluids are maintained even after long periods of storage or use.

Various methods of maintaining the stability of nanofluids or colloidal suspensions have been used in experiments to try and maintain the stability for extended periods of time. Some of the methods included the use of surfactants or stabilising agents, the production of a nanofluid with a high zeta potential exceeding values of +/-30 mV and monitoring the pH of a solution to give electrostatic repulsion [7, 144-149]. Several literature reports have also mentioned the use of sonification to break down any agglomerates that are present from the production of the nanofluid and also give rise to a more homogeneous mixture. Whilst sonification can break down the initial agglomerates present in the nanofluid, it only temporarily slows down the formation of aggregates unless other stabilising methods are used [55, 146, 150, 151].

When measuring the stability of a nanofluid it is key to be able to characterise how well the particles are dispersed through the base fluid, Yu et al. [152] introduced a figure which shows methods to characterise and determine the stability of a nanofluid (Figure 5) although the methods shown in the figure are not conclusive, they are the most common methods currently used.

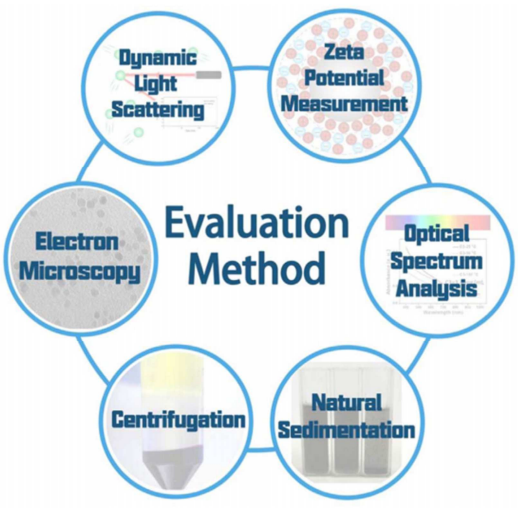

Figure 5. *The most common methods used to characterise and determine the stability of a nanofluid. Adopted from [152].*

In 2012 Lee et al. [111] had prepared a stable solution of a magnetite/water nanofluid with a volume concentration of 100 ppm, stating that the zeta potential was above 30 mV (approximately 38 mV) meaning the suspension was stable and that the zeta potential decreased over time to around 30 mV after a period of 24 hours. Although there is a distinct lack of long-term experiments to determine the stability of nanofluids, Lee et al. [73] performed an experiment using a magnetite/water nanofluid. The nanofluid was created using a two-step method and was also sonicated to improve the suspension stability and break down aggregates. The experiment was performed over a two-year period to determine the effect that storage time of a nanofluid had on the CHF for possible applications in the nuclear industry. A dilution process to allow the storage of nanofluids was proposed, although it was noted that the effects of dilution on the CHF were unknown. It was concluded that the CHF enhancement of the nanofluid can be guaranteed until an approximate concentration of 1000 ppm for a minimum time period of 1 year, after which the CHF gradually decreased over time.

Kole and Dey [153] performed experiments to determine the effects that the sonication time had on the agglomerate diameter at various concentrations and temperatures. A ZnO/Ethylene Glycol nanofluid was used and characterised using TEM which showed that the particles were spherical and had an average diameter of < 50 nm. Once dispersed in the ethylene glycol with volume fractions of 0.005 and 0.0375%, dynamic light scattering was used to measure the average aggregate diameter, which was between 90 and 154 nm. A suspension with a volume fraction of 0.01% was prepared and sonication performed between 4 and 100 hours. It was found that the size of the aggregates rapidly decreased from 459 nm to approximately 91 nm between 4 and 60 hours, the average cluster size then increased up until the 100-hour mark depicted in Figure 6.

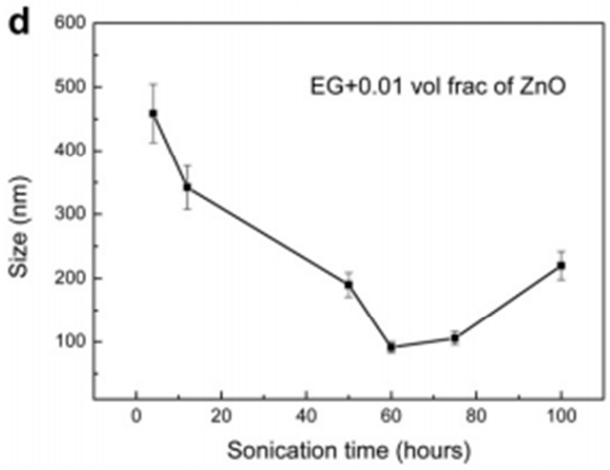

Figure 6. *A depiction of the cluster size of a ZnO nanofluid of volume fraction 0.01 after various sonication times. Adopted from [153].*

Although Kole and Dey performed experiments showing

that the average particle size decreased as sonification time increased, Yu et al. [154] performed experiments using a Fe_3O_4/kerosene in which the Fe_3O_4 had previously had oleic acid chemisorbed to the surface to allow for compatibility with the kerosene. They reported that the average particle diameter before placing the Iron Oxide in the kerosene was 15 nm and an average cluster size of 155 nm when placed in the kerosene. Contrary to the work of Kole and Dey, it was reported that no clear relationship between the cluster size and ultrasonication time could be found.

5. Conclusion

Nanoparticles have been widely demonstrated by experiments to be able to enhance the thermal conductivity, convective heat transfer and CHF of the base fluids when mixed with them. By how much this enhancement can be made depends on the concentration and characteristics of nanoparticles used and the stability of the nanofluids. These characteristics are referring to the type, size and shape of the nanoparticles. To this end, mathematical models have been attempted for various circumstances to at least describe experimental data; nevertheless, there is so far no general agreement to which model has its general applicability even to each of the three types of enhancement. Most of work still remains on the stage of experimenting – trial and error. Understanding of the mechanisms is still a myth. This indicates that there is a strong need for a fundamental development of nanoparticle enhancing heat transfer in an integrated way so that each type of the enhancements is regarded as only a way that how nanoparticles express themselves under different operating conditions – this sounds quite philosophical but remains to be a realistic challenge for research in this area to take a significant step forward.

As for the CHF, the aspect that this review is mostly concerned about, enhancements up to 300% for non-hybrid and 700% for hybrid nanofluids have been found. Studies have shown that the orientation and structure of heating surface also have effects on the CHF enhancement. Increasing the inclining angle and adding porous structure onto heating surfaces will both increase the CHF enhancement. Nanoparticle deposition onto the heating surface to increase the nucleate pool boiling is sound a way to explain in general this type of enhancement. However, reducing contact angle and increasing capillary wicking come to play the roles to explain the heat surface effects respectively as mentioned above. The Zuber correlation and Kandllikar's model were discussed to reasonably agree with some experimental data of the CHF enhancement among other models for different circumstances.

Stability particularly long-term (more than a year) stability appears to be a major obstacle that hinders the way of nanofluids' industrial application especially under pool boiling conditions. Chemical stabilisation (measured by zeta potential), polymer stabilisation (measured by the concentration of the polymer used) and sonication (measured by time) seem to be the most common ways to stabilise nanofluids in lab scale, while the chemical stabilisation method seems holding its place as the most favourable one as it is less affected by the operating conditions such as temperature. However, these methods under the real working environment have not been investigated. This stability issue is an area that has to be addressed before any application of nanofluids in heat transfer enhancement in an industrial scale can be made in a near future.

6. Challenges and Research Direction

The main challenge that lies ahead in the field of nanoparticle enhancing heat transfer is that the mechanism how the enhancement is taking place is still unclear. Without established understanding of the mechanism, control and improvement would not be possible. A significant amount of research is yet needed to establish a robust quantitative relationship between the enhanced heat transfer properties and the properties of nanoparticles (such as size, shape and other physical properties) and the base fluids (thermal conductivity and viscosity, etc). The enhanced heat transfer properties refer to the convective and critical heat transfer coefficients not only the thermal conductivity.

The long-term stability of nanofluids is also a large issue and requires further research as it is key to have the stability and enhanced properties of the nanofluids remaining consistent, even under extreme conditions such as boiling. Once the long-term stability and enhanced properties of nanofluids can be maintained for long periods of time, it will become more likely that they will be able to be applied to engineering applications in the future. Models will need to be established to predict the lifetime of a nanofluid to allow for industrialisation as a new heat transfer medium, as there are currently very few studies that have observed the long-term stability of a nanofluid with no proven models present.

Rigorous characterisation techniques that will be able to give the real time information of the dispersion state of the nanoparticles in fluids are highly desirable as this will not only monitor the nanoparticles in processing but also provides a way to justify the operational period of the particles. Besides that, they are essential to underpin any further proposed physical models and mechanisms.

Another area requiring development is a database of nanofluid types with varying base fluids and types of nanoparticles such as oxides, metals and compounds to allow for quick reference of expected values for the enhancement that is possible. This will allow a faster route to determine which nanofluids are more suitable to specific applications based on the enhancement of properties, the stability time and the cost of production.

Acknowledgements

The funding from the Engineering and Physical Sciences Council (EPSRC) of UK for a doctor training partnership with the University of Huddersfield is gratefully acknowledged.

Nomenclature

(Note, symbols not listed in the following table can be found explained in the context)

Symbols	
C	A constant in Kumar's model equation for thermal conductivity (kg K^{-1} s^{-2})
g	Gravitational acceleration (m^2 s^{-1})
G	Mass flux (kg m^{-2} s^{-1})
h_{lv}	Enthalpy of vaporisation (J kg^{-1})
h_t	Thickness of the interfacial layer (m)
k	thermal conductivity (W m^{-1} K^{-1})
k_{ad}	Adsorbed thermal conductivity (W m^{-1} K^{-1})
k_B	Boltzmann constant (J K^{-1})
k_{cp}	Thermal conductivity of clustered particles (W m^{-1} K^{-1})
k_{lr}	Thermal conductivity of the interfacial layer on the surface of particles (W m^{-1} K^{-1})
$k_{Maxwell}$	Thermal conductivity calculated by the Maxwell equation (W m^{-1} K^{-1})
Pe	Peclet number (-)
Pr	Prandtl number (-)
r_b	Radius of fluid layer on the surface of nanoparticles in Kumar's model for thermal conductivity (m)
Re	Reynolds number (-)
S	Smoothing factor allowing Kandlikar's equation to fit smooth surfaces (-)
T_b	Boiling temperature (°C)
T_s	Saturated temperature (°C)
T_∞	Bulk temperature (°C)
ΔT_{sub}	Change in subcooled temperature (°C)
ϵ	Porosity (-)
ϕ	Heater orientation angle (°)
φ	Volume concentration of the nanoparticles (-)
γ	Ratio of interfacial layer thickness and particle radius (-)
$\gamma_1 = 1 + \gamma/2$	
μ	Viscosity (Pa s)
σ	Surface tension (N m^{-1})
θ	Contact angle (°)
Subscripts	
bf	Base fluid
l	Liquid
lv	Liquid/vapour interface
nf	Nanofluid
p	Particle
r	Relative (to base fluid in most cases)
v	Vapour

References

[1] S. Choi, Enhancing thermal conductivity of fluids with nanoparticles, in American Society of Mechanical Engineers, Fluids Engineering Division (Publication) FED, San Francisco, 99-105, 1995.

[2] T. T. Baby and S. Ramaprabhu, Experimental investigation of the thermal transport properties of a carbon nanohybrid dispersed nanofluid, Nanoscale 3 (2011) 2208-2214.

[3] H. Akoh, Y. Tsukasaki, S. Yatsuya, and A. Tasaki, Magnetic properties of ferromagnetic ultrafine particles prepared by vacuum evaporation on running oil substrate, Journal of Crystal Growth 45 (1978) 495-500.

[4] H.-t. Zhu, Y.-s. Lin, and Y.-s. Yin, A novel one-step chemical ethod for preparation of copper nanofluids, Journal of Colloid and Interface Science 277 (2004) 100-103.

[5] D. K. Devendiran and V. A. Amirtham, A Review on Preparation, Characterization, Properties and Applications of Nanofluids, Renewable and Sustainable Energy Reviews 60 (2016) 21-40.

[6] D. K. Devendiran and V. A. Amirtham, A Comprehensive Review of Preparation, Characterization, Properties and Stability of Hybrid Nanofluids, Renewable and Sustainable Energy Reviews (2017).

[7] G. Paul, P. K. Das, and I. Manna, Synthesis, Characterization and Studies on Magneto-viscous Properties of Magnetite Dispersed Water Based Nanofluids, Journal of Magnetism and Magnetic Materials 404 (2016) 29-39.

[8] A. Ghadimi, R. Saidur, and H. S. C. Metselaar, A Review of Nanofluid Stability Properties and Characterization in Stationary Conditions, International Journal of Heat and Mass Transfer 54 (2011) 4051-4068.

[9] M. B. Moghaddam, E. K. Goharshadi, M. H. Entezari, and P. Nancarrow, Preparation, Characterization, and Rheological Properties of Graphene-Glycerol Nanofluids, Chemical Engineering Journal 231 (2013) 365-372.

[10] R. M. Sarviya and V. Fuskele, Review on Thermal Conductivity of Nanofluids, Materials Today: Proceedings 4 (2017) 4022-4031.

[11] R. L. Hamilton and O. K. Crosser, Thermal conductivity of heterogeneous two-component systems, Ind. Eng. Chem. Fundam. 1 (1962) 187.

[12] J. C. Maxwell, Electricity and Magnetism, Vol. 1. Clarendon Press, Oxford, UK, 1873.

[13] D. J. Jeffrey, Conduction through a random suspension of spheres, Proceedings of the Royal Society A: Mathematical, Physical & Engineering Sciences 335 (1602) (1973) 355-367.

[14] W. Yu and S. U. S. Choi, The role of interfacial layers in the enhanced thermal conductivity of nanofluids: a renovated Maxwell model, J. Nanopart. Res. 5 (2003) 167.

[15] S. A Angayarkanni and J. Philip, Review on thermal properties of nanofluids: Recent developments, Advances in Colloid and Interface Science 225 (2015) 146-176.

[16] J. C. Maxwell, A treatise on electricity and magnetism, 2nd ed ed. Clarendon Press, 1881.

[17] D. A. G. Bruggeman, Berechnung verschiedener physikalischer Konstanten von heterogenen Substanzen. I. Dielektrizitätskonstanten und Leitfähigkeiten der Mischkörper aus isotropen Substanzen, Annalen der Physik 416 (7) (1935).

[18] W. Yu and S. U. S. Choi, The role of interfacial layers in the enhanced thermal conductivity of nanofluids: A renovated Hamilton–Crosser model, Journal of Nanoparticle Research 6 (4) (2004) 355-361.

[19] Z. Hashin and S. Shtrikman, A Variational Approach to the Theory of the Effective Magnetic Permeability of Multiphase Materials, Journal of Applied Physics 33 (10) (1962).

[20] J. Avsec and M. Oblak, The calculation of thermal conductivity, viscosity and thermodynamic properties for nanofluids on the basis of statistical nanomechanics, International Journal of Heat and Mass Transfer 50 (21-22) (2007) 4331-4341.

[21] X. Yimin and Q. Li, Investigation on Convective Heat Transfer and Flow Features of Nanofluids, Journal of Heat Transfer 125 (1) (2003) 151-155.

[22] B. C. Pak and Y. I. Cho, Hydrodynamic and heat transfer study of dispersed fluids with submicron metallic oxide particles, Experimental Heat Transfer 11 (2) (1998) 151-170.

[23] D. H. Kumar, H. E. Patel, V. R. R. Kumar, T. Sundararajan, T. Pradeep, and S. K. Das, Model for Heat Conduction in Nanofluids, Physical Review Letters 93 (2004) 144301.

[24] M. Chandrasekar, S. Suresh, R. Srinivasan, and A. C. Bose, New Analytical Models to Investigate Thermal Conductivity of Nanofluids, Journal of Nanoscience and Nanotechnology 9 (1) (2009) 533-538.

[25] R. Prasher, P. Bhattacharya, and P. E. Phelan, Thermal Conductivity of Nanoscale Colloidal Solutions (Nanofluids), Physical Review Letters 94 (2005) 025901.

[26] K. C. Leong, C. Yang, and S. M. S. Murshed, A model for the thermal conductivity of nanofluids – the effect of interfacial layer, Journal of Nanoparticle Research 8 (2) (2006) 245-254.

[27] E. Yamada and T. Ota, Effective thermal conductivity of dispersed materials, Wärme - und Stoffübertragung 13 (1-2) (1980) 27-37.

[28] S. K. Gupta, S. G. Advani, and P. Huq, Role of Micro-convection due to nonaffine motion of particle in mono-disperse suspension, International Journal of Heat and Mass Transfer 38 (2945-2958) (1995).

[29] D. P. H. Hesselman and L. F. Johnson, Effective thermal conductivity of nanocomposites with interfacial thermal barrier resistance, Journal of Composite Materials 21 (1987) 508-515.

[30] H. Xie, M. Fujii, and X. Zhang, Effect of interfacial nanolayer on the effective thermal conductivity of nanoparticle-fluid mixture, International Journal of Heat and Mass Transfer 48 (14) (2005) 2926-2932.

[31] S. P. Jang and S. U. Choi, Role of Brownian Motion in the Enhanced Thermal Conductivity of Nanofluids, Appl. Phys. Lett. 84 (21) (2004) 4316-4318.

[32] E. V. Timofeeva, A. N. Gavrilov, J. M. McCloskey, Y. V. Tolmachev, S. Sprunt, L. M. Lopatina, and J. V. Selinger, Thermal conductivity and particle agglomeration in alumina nanofluids: Experiment and theory, Physical Review E 76 (2007).

[33] B.-X. Wang, L.-P. Zhou, and X.-F. Peng, A fractal model for predicting the effective thermal conductivity of liquid with suspension of nanoparticles, International Journal of Heat and Mass Transfer 46 (14) (2003) 2665-2672.

[34] M. E. Meibodi, M. V. Sefti, A. M. Rashidi, A. Amrollahi, M. Tabasi, and H. S. Kalal, A model for thermal conductivity of nanofluids, Mater. Chem Phys 123 (2010) 639-643.

[35] W. Wang, L. Lin, Z. X. Feng, and S. Y. Wang, A comprehensive model for enahnced thermal conductivity of nanofluids, J. Adv. Res Phys 3 (2012).

[36] M. Corcione, Empirical correlating equations for predicting the effective thermal conductivity and dynamic viscosity of nanofluids, Energy Conversion and Management 52 (1) (2011) 789-793.

[37] B.-X. Wang, W.-Y. Sheng, and X.-F. Peng, A Novel Statistical Clustering Model for Predicting Thermal Conductivity of Nanofluid, International Journal of Thermophysics 30 (2009).

[38] C. H. K. Chon, Kenneth D. Lee, S. P. Choi, and S. U. S., Empirical correlation finding the role of temperature and particle size for nanofluid (Al_2O_3) thermal conductivity enhancement, Appl. Phys. Lett. 87 (2005) 153107.

[39] K. D. Kihm, C. H. Chon, J. S. Lee, and S. U. S. Choi, A new heat propagation velocity prevails over Brownian particle velocities in determining the thermal conductivities of nanofluids, Nanoscale Research Letters 6 (2011) 1-9.

[40] W. Evans, Role of Brownian motion hydrodynamics on nanofluid thermal conductivity, Applied Physics Letters 88 (2006).

[41] W. Evans, R. Prasher, J. Fish, P. Meakin, P. Phelan, and P. Keblinski, Effect of aggregation and interfacial thermal resistance on thermal conductivity of nanocomposites and colloidal nanofluids, International Journal of Heat and Mass Transfer 51 (5-6) (2008).

[42] B. Yang, Thermal Conductivity Equations Based on Brownian Motion in Suspensions of Nanoparticles (Nanofluids), Journal of Heat Transfer 130 (4) (2008).

[43] L. Braginsky and V. Shklover, Thermal conductivity of low-particle-concentration suspensions: Correlation function approach, PHYSICAL REVIEW B 78 (2008).

[44] R. S. Vajjha and D. K. Das, Experimental determination of thermal conductivity of three nanofluids and development of new correlations, International Journal of Heat and Mass Transfer 52 (21-22) (2009) 4675-4682.

[45] C. J. Ho, L. C. Wei, and Z. W. Li, An experimental investigation of forced convective cooling performance of a microchannel heat sink with Al_2O_3/water nanofluid, Applied Thermal Engineering 30 (2-3) (2010) 96-103.

[46] S. Kakaç and A. Pramuanjaroenkij, Review of convective heat transfer enhancement with nanofluids, International Journal of Heat and Mass Transfer 52 (13) (2009) 3187-3196.

[47] M. Vegad, S. Satadia, P. Pradip, P. Chirag, and P. Bhargav, Heat transfer characteristics of low Reynolds number flow of nanofluid around a heated circular cylinder, Procedia Technology 14 (2014) 348-356.

[48] A. A. Minea and G. Lorenzini, A numerical study of ZnO based nanofluids behavior on natural convection, International Journal of Heat and Mass Transfer 114 (2017) 286-296.

[49] T. Okawa, K. Nagano, and T. Hirano, Boiling heat transfer during single nanofluid drop impacts onto a hot wall, Experimental Thermal and Fluid Science 36 (2011) 78-85.

[50] H. Lotfi and M. B. Shafii, Boiling heat transfer on a high temperature silver sphere in nanofluid, International Journal of Thermal Sciences 48 (2009) 2215-2220.

[51] S. Vafaei, Nanofluid pool boiling heat transfer phenomenon, Powder Technology 277 (2015) 181-192.

[52] S. H. Noie, S. Z. Heris, M. Kahani, and S. M. Nowee, Heat transfer enhancement using Al_2O_3/water nanofluid in a two-phase closed thermosyphon, International Journal of Heat and Fluid Flow 30 (2009) 700-705.

[53] R. Kathiravan, R. Kumar, A. Gupta, R. Chandra, and P. K. Jain, Pool boiling characteristics of multiwalled carbon nanotube (CNT) based nanofluids over a flat plate heater, International Journal of Heat and Mass Transfer 54 (2011) 1289-1296.

[54] K. H. Do, H. J. Ha, and S. P. Jang, Thermal resistance of screen mesh wick heat pipes using the water-based Al_2O_3 nanofluids, International Journal of Heat and Mass Transfer 53 (2010) 5888-5894.

[55] D. Wen, M. Corr, X. Hu, and G. Lin, Boiling heat transfer of nanofluids: The effect of heating surface modification, International Journal of Thermal Sciences 50 (2011) 480-485.

[56] H. D. Kim, J. Kim, and M. H. Kim, Effect of nanoparticles on CHF enhancement in pool boiling of nano-fluids, International Journal of Heat and Mass Transfer 49 (2006) 5070-5074.

[57] S. Khandekar, Y. M. Joshi, and B. Mehta, Thermal performance of closed two-phase thermosyphon using nanofluids, International Journal of Thermal Sciences 47 (2008) 659-667.

[58] J. S. Coursey and J. Kim, Nanofluid boiling: The effect of surface wettability, International Journal of Heat and Fluid Flow 29 (2008) 1577-1585.

[59] M. N. Golubovic, H. H. D. M., W. M. Worek, and W. J. Minkowycz, Nanofluids and critical heat flux, experimental and analytical study, Applied Thermal Engineering 29 (2009) 1281-1288.

[60] H. S. Ahn, S. H. Kang, C. Lee, J. Kim, and M. H. Kim, The effect of liquid spreading due to micro-structures of flow boiling critical heat flux, International Journal of Multiphase Flow 43 (2012) 1-12.

[61] E. Forrest, E. Williamson, J. Buorgiorno, L.-W. Hu, M. Rubner, and R. Cohen, Augmentation of nucleate boiling heat transfer and critical heat flux using nanoparticle thin-film coatings, International Journal of Heat and Mass Transfer 53 (2010) 58-67.

[62] S. Kim, H. D. Kim, H. Kim, H. S. Ahn, H. Jo, J. Kim, and M. H. Kim, Effects of nano-fluid and surfaces with nano structure on the increase of CHF, Experimental Thermal and Fluid Science 34 (2010) 487-495.

[63] S. K. Verma and A. K. Tiwari, Characterization of Nanofluids as an Advanced Heat Transporting Medium for Energy Systems, Materials Today: Proceedings 4 (2017) 4095-4103.

[64] M. Amani, P. Amani, A. Kasaeian, O. Mahian, and W.-M. Yan, Two-phase mixture model for nanofluid turbulent flow and heat transfer: Effect of heterogeneous distribution of nanoparticles, Chemical Engineering Science 167 (2017) 135-144.

[65] R. V. Pinto and F. A. S. Fiorelli, Review of the mechanisms responsible for heat transfer enhancement using nanofluids, Applied Thermal Engineering 108 (2016) 720-739.

[66] D. M. Vazquez and R. Kumar, Surface effects of ribbon heaters on critical heat flux in nanofluid pool boiling, International Communications in Heat and Mass Transfer 41 (2013) 1-9.

[67] J. H. Kim, J. M. Kim, D. W. Jerng, E. Y. Kim, and H. S. Ahn, Effect of aluminum oxide and reduced graphene oxide mixtures on critical heat flux enhancement, International Journal of Heat and Mass Transfer 116 (2018) 858-870.

[68] N. Zuber, On the stability of boiling heat transfer, Trans. Am. Soc. Mech. Engrs. 80 (1958) 711-720.

[69] M. Dadjoo, N. Etesami, and M. N. Esfahany, Influence of orientation and roughness of heater surface on critical heat flux and pool boiling heat transfer coefficient of nanofluid, Applied Thermal Engineering 124 (2017) 353-361.

[70] S. D. Park, S. B. Moon, and I. C. Bang, Effects of thickness of boiling-induced nanoparticle deposition on the saturation of critical heat flux enhancement, International Journal of Heat and Mass Transfer 78 (2014) 506-514.

[71] H. S. Ahn and M. H. Kim, The boiling phenomenon of alumina nanofluid near critical heat flux, international Journal of Heat and Mass Transfer 62 (2013) 718-729.

[72] R. A. Neto, J. L. G. Oliveira, and J. C. Passos, Heat transfer coefficient and critical heat flux during nucleate pool boiling of water in the presence of nanoparticles of alumina maghemite and CNTs, Applied Thermal Engineering 111 (2017) 1493-1506.

[73] J. H. Lee, D. H. Kam, and Y. H. Jeong, The effect of nanofluid stability on critical heat flux using magnetite-water nanofluids, Nuclear Engineering and Design 292 (2015) 187-192.

[74] R. Kamatchi and S. Venkatachalapathy, Parametric study of pool boiling heat transfer with nanofluids for enhancement of critical heat flux: A review, International Journal of Thermal Sciences 87 (2015) 228-240.

[75] X. Fang, Y. Chen, H. Zhang, W. Chen, A. Dong, and R. Wang, Heat transfer and critical heat flux of nanofluid boiling: A comprehensive review, Renewable and Sustainable Energy Reviews 62 (2016) 924-940.

[76] S. G. Kandlikar, A Theoretical Model to Predict Pool Boiling CHF Incorporating Effects of Contact Angle and Orientation, Journal of Heat Transfer 123 (2001) 1071-1079.

[77] D. H. Kam, Y. J. Choi, and Y. H. Jeong, Critical heat flux on downward-facing carbon steel flat plates under atmospheric condition, Experimental Thermal and Fluid Science 90 (2018) 22-27.

[78] H. T. Phan, R. Bertossi, N. Caney, P. Marty, and S. Colassan, A model to predict the effect of surface wettability on critical heat flux, International Communications in Heat and Mass Transfer 39 (2012) 1500-1504.

[79] Y. J. Choi, D. H. Kam, and Y. H. Jeong, Analysis of CHF enhancement by magnetite nanoparticle deposition in the subcooled flow boiling region, International Journal of Heat and Mass Transfer 109 (2017) 1191-1199.

[80] R. Li and Z. Huang, A new CHF model for enhanced pool boiling heat transfer on surfaces with micro-scale roughness, International Journal of Heat and Mass Transfer 109 (2017) 1084-1093.

[81] H. S. Ahn, C. Lee, J. Kim, and M. H. Kim, The effect of capillary wicking action of micro/nano structures on pool boiling critical heat flux, International Journal of Heat and Mass Transfer 55 (2012) 89-92.

[82] S.-S. Park, Y. H. Kim, Y. H. Jeon, M. T. Hyun, and N.-J. Kim, Effects of spray-deposited oxidized multi-wall carbon nanotubes and graphene on pool-boiling critical heat flux enhancement, Journal of Industrial and Engineering Chemistry 24 (2015) 276-283.

[83] S. Mori, S. M. Aznam, and K. Okuyama, Enhancement of the critical heat flux in saturated pool boiling of water by nanoparticle-coating and a honeycomb porous plate, International Journal of Heat and Mass Transfer 80 (2015) 1-6.

[84] S. M. Aznam, S. Mori, A. Ogoshi, and K. Okuyama, CHF enhancement of a large heated surface by a honeycomb porous plate and a gridded metal structure in a saturated pool boiling of nanofluid, International Journal of Heat and Mass Transfer 115 (2017) 969-980.

[85] S. Mori and Y. Utaka, Critical heat flux enhancement by surface modification in a saturated pool boiling: A review, International Journal of Heat and Mass Transfer 108 (2017) 2534-2557.

[86] S. L. Song and S. H. Chang, An experimental study on CHF enhancement of wire nets covered surface in R-134a flow boiling under high pressure and high mass flux conditions, International Journal of Heat and Mass Transfer 90 (2015) 761-768.

[87] V. Saeid and W. Dongsheng, Critical heat flux of nanofluids inside a single microchannel: Experiments and correlations, Chemical Engineering Research and Design 92 (2014) 2339-2351.

[88] H. S. Ahn, H. D. Kim, H. J. Jo, S. H. Kang, W. P. Chang, and M. H. Kim, Experimental study of critical heat flux enhancement during forced convective flow boiling of nanofluid on a short heated surface, International Journal of Multiphase Flow 36 (2010) 375-384.

[89] A. Mourgues, V. Hourtané, T. Muller, and M. Caron-Charles, Boiling behaviors and critical heat flux on a horizontal and vertical plate in saturated pool boiling with and without ZnO nanofluid, International Journal of Heat and Mass Transfer 57 (2013) 595-607.

[90] H. S. Ahn, J. M. Kim, J. M. Kim, S. C. Park, K. Hwang, H. J. Jo, T. Kim, D. W. Jerng, M. Kaviany, and M. H. Kim, Boiling characteristics on the reduced graphene oxide films, Experimental Thermal and Fluid Science 60 (2015) 361-366.

[91] C.-K. Huang, C.-W. Lee, and C.-K. Wang, Boiling enhancement by TiO_2 nanoparticle deposition, International Journal of Heat and Mass Transfer 54 (2011) 4895-4903.

[92] S. L. Song, J. H. Lee, and S. H. Chang, CHF enhancement of SiC nanofluid in pool boiling experiment, Experimental Thermal and Fluid Science 52 (2014) 12-18.

[93] G. M. Son, K. M. Kim, and I. C. Bang, Chromia coating with nanofluid deposition and sputtering for accident tolerance, CHF enhancement, International Journal of Heat and Mass Transfer 118 (2018) 890-899.

[94] S. W. Lee, S. D. Park, and I. C. Bang, Critical heat flux for CuO nanofluid fabricated by pulsed laser ablation differentiating deposition characteristics, International Journal of Heat and Mass Transfer 55 (2012) 6908-6915.

[95] E. dos Santos Filho, F. J. dos Nascimento, D. C. Moreira, and G. Ribatski, Dynamic wettability evaluation of nanoparticles-coated surfaces, Experimental Thermal and Fluid Science 92 (2018) 231-242.

[96] H. D. Kim, E. Kim, and M. H. Kim, Effect of nanoparticle deposit layer properties on pool boiling critical heat flux of water from a thin wire, International Journal of Heat and Mass Transfer 69 (2014) 164-172.

[97] S. D. Park, S. W. Lee, S. Kang, S. M. Kim, H. Seo, and I. C. Bang, Effects of Al_2O_3/R-123 nanofluids containing $C_{19}H_{40}$ core–shell phase change materials on critical heat flux, International Journal of Heat and Mass Transfer 55 (2012) 7144-7150.

[98] G. H. Seo, U. Jeong, H. H. Son, D. Shin, and S. J. Kim, Effects of layer-by-layer assembled PEI/MWCNT surfaces on enhanced pool boiling critical heat flux, International Journal of Heat and Mass Transfer 109 (2017) 564-576.

[99] Y. Hu, Z. Liu, and Y. He, Effects of SiO_2 nanoparticles on pool boiling heat transfer characteristics of water based nanofluids in a cylindrical vessel, Powder Technology 327 (2018) 79-88.

[100] M. Meier, J. Ungerer, M. Klinge, and H. Nirschl, Synthesis of nanometric silica particles via a modified Stober synthesis route, Colloids and Surfaces A 538 (2018) 559-564.

[101] Q. T. Pham, T. I. Kim, S. S. Lee, and S. H. Chang, Enhancement of critical heat flux using nano-fluids for Invessel Retention-External Vessel Cooling, Applied Thermal Engineering 35 (2012) 157-165.

[102] V. I. Sharma, J. Buongiorno, T. J. McKrell, and L. W. Hu, Experimental investigation of transient critical heat flux of water-based zinc–oxide nanofluids, International Journal of Heat and Mass Transfer 61 (2013) 425-431.

[103] S. D. Park and I. C. Bang, Experimental study of a universal CHF enhancement mechanism in nanofluids using hydrodynamic instability, International Journal of Heat and Mass Transfer 70 (2014) 844-850.

[104] E. J. Park, S. D. Park, I. C. Bang, Y.-B. Park, and H. W. Park, Critical heat flux characteristics of nanofluids based on exfoliated graphite nanoplatelets (xGnPs), Materials Letters 81 (2012) 193-197.

[105] W. S. Hummers Jr and R. E. Offeman, Preparation of Graphitic Oxide, J. Am. Chem. Soc 80 (6) (1958) 1339.

[106] E. J. Park, I. C. Bang, and H. W. Park, Experimental observation of the critical heat flux (CHF) enhancement of the nanofluids by the electrical explosion of a wire in liquid, International Journal of Heat and Mass Transfer 79 (2014) 868-875.

[107] S. W. Lee, K. M. Kim, and I. C. Bang, Study on flow boiling critical heat flux enhancement of graphene oxide/water nanofluid, International Journal of Heat and Mass Transfer 65 (2013) 348-356.

[108] G. Dewitt, T. J. McKrell, J. Buongiorno, L. W. Hu, and R. J. Park, Experimental study of critical heat flux with alumina-water nanofluids in downward-facing channels for in-vessel retention applications, Nuclear Engineering and Technology 45 (3) (2013).

[109] H. S. Ahn, J. M. Kim, and M. H. Kim, Experimental study of the effect of a reduced graphene oxide coating on critical heat flux enhancement, International Journal of Heat and Mass Transfer 60 (2013) 763-771.

[110] R. K. Cheedarala, E. Park, K. Kong, Y.-B. Park, and H. W. Park, Experimental study on critical heat flux of highly efficient soft hydrophilic CuO–chitosan nanofluid templates, International Journal of Heat and Mass Transfer 100 (2016) 396-406.

[111] J. H. Lee, T. Lee, and Y. H. Jeong, Experimental study on the pool boiling CHF enhancement using magnetite-water nanofluids, International Journal of Heat and Mass Transfer (2012) 2656-2663.

[112] S. D. Park and I. C. Bang, Flow boiling CHF enhancement in an external reactor vessel cooling (ERVC) channel using graphene oxide nanofluid, Nuclear Engineering and Design 265 (2013) 310-318.

[113] T. I. Kim, W. J. Chang, and S. H. Chang, Flow boiling CHF enhancement using Al_2O_3 nanofluid and an Al_2O_3 nanoparticle deposited tube, International Journal of Heat and Mass Transfer 54 (2011) 2021-2025.

[114] T. Lee., J. H. Lee, and Y. H. Jeong, Flow boiling critical heat flux characteristics of magnetic nanofluid at atmospheric pressure and low mass flux conditions, International Journal of Heat and Mass Transfer 56 (2013) 101-106.

[115] J. L. G. O. A. Rainho Neto, J. C Passos, Heat transfer coefficient and critical heat flux during nucleate pool boiling of water in the presence of nanoparticles of alumina, maghemite and CNTs, Applied Thermal Engineering 111 (2017) 1493-1506.

[116] R. Kamatchi and G. Kumaresan, Investigations on pool boiling critical heat flux, transient characteristics and bonding strength of heater wire with aqua based reduced graphene oxide nanofluids, Chinese Journal of Chemical Engineering 26 (2018) 445-454.

[117] M. Kole and T. K. Dey, Investigations on the pool boiling heat transfer and critical heat flux of ZnO-ethylene glycol nanofluids, Applied Thermal Engineering 37 (2012) 112-119.

[118] K.-J. Park, D. Jung, and S. E. Shim, Nucleate boiling heat transfer in aqueous solutions with carbon nanotubes up to critical heat fluxes, International Journal of Multiphase Flow 35 (2009) 525-532.

[119] J. M. Kim, J. H. Kim, S. C. Park, M. H. Kim, and H. S. Ahn, Nucleate boiling in graphene oxide colloids: Morphological change and critical heat flux enhancement, International Journal of Multiphase Flow 85 (2016) 209-222.

[120] S. M. Kwark, R. Kumar, G. Moreno, J. Yoo, and S. M. You, Pool boiling characteristics of low concentration nanofluids, International Journal of Heat and Mass Transfer 53 (2010) 972-981.

[121] S. D. Park, S. W. Lee, S. Kang, S. M. Kim, and I. C. Bang, Pool boiling CHF enhancement by graphene-oxide nanofluid under nuclear coolant chemical environments, Nuclear Engineering and Design 252 (2012) 184-191.

[122] H. S. Ahn, J. M. Kim, M. Kaviany, and M. H. Kim, Pool boiling experiments in reduced graphene oxide colloids. Part I – Boiling characteristics, International Journal of Heat and Mass Transfer 74 (2014) 501-512.

[123] A. Amiri, M. Shanbedi, A. H., S. Zerinali Heris, S. N. Kazi, B. T. Chew, and H. Eshghi, Pool boiling heat transfer of CNT/water nanofluids, Applied Thermal Engineering 71 (2014) 450-459.

[124] J.-Y. Jung, E. S. Kim, and Y. T. Kang, Stabilizer effect on CHF and boiling heat transfer coefficient of alumina/water nanofluids, International Journal of Heat and Mass Transfer 55 (2012) 1941-1946.

[125] S. J. Kim, I. C. Bang, J. Buongiorno, and L. W. Hu, Surface wettability change during pool boiling of nanofluids and its effect on critical heat flux, International Journal of Heat and Mass Transfer 50 (2007) 4105-4116.

[126] Y. Wang, K. Deng, J. Wu, G. Su, and S. Qiu, The characteristics and correlation of nanofluid flow boiling critical heat flux, International Journal of Heat and Mass Transfer 122 (2018) 212-221.

[127] G. Liang and I. Mudawar, Pool boiling critical heat flux (CHF) - Part 2: Assessment of models and correlations, International Journal of Heat and Mass Transfer (2017).

[128] S. S. Kutateladze, On the transition to film boiling under natural convection, Kotloturbostroenie 3 (3) (1948) 10-12.

[129] J. H. Lienhard and V. K. Dhir, Hydrodynamic Prediction of Peak Pool-boiling Heat Fluxes from Finite Bodies, Journal of Heat Transfer 95 (2) (1973) 152-158.

[130] L. Wang, Y. Li, F. Zhang, F. Xie, and Y. Ma, Correlations for calculating heat transfer of hydrogen pool boiling, International Journal of Hydrogen Energy 41 (38) (2016) 17118-31.

[131] W. M. Rohsenow and P. Griffith, Correlation of maximum heat transfer data for boiling of saturated liquids, Chem. Eng. Prog. Symp. Ser. 52 (1955) 47-49.

[132] Y. Haramura and Y. Katto, A new hydrodynamic model of critical heat flux, applicable widely to both pool and forced convection boiling on submerged bodies in saturated liquids, International Journal of Heat and Mass Transfer 26 (3) (1983) 389-399.

[133] V. V. Yagov, Is a crisis in pool boiling actually a hydrodynamic phenomenon?, International Journal of Heat and Mass Transfer 73 (2014) 265-273.

[134] C.-K. Guan, J. F. Klausner, and R. Mei, A new mechanistic model for pool boiling CHF on horizontal surfaces, International Journal of Heat and Mass Transfer 54 (17-18) (2011) 3960-3969.

[135] I. Mudawar, A. H. Howard, and C. O. Gersey, An analytical model for near-saturated pool boiling critical heat flux on vertical surfaces, International Journal of Heat and Mass Transfer 40 (10) (1997) 2327-2339.

[136] M. S. El-Genk and H. Bostanci, Saturation boiling of HFE-7100 from a copper surface, simulating a microelectronic chip, International Journal of Heat and Mass Transfer 46 (10) (2003) 1842-1854.

[137] I. P. Vishnev, Effect of orienting the hot surface with respect to the gravitational field on the critical nucleate boiling of a liquid, Journal of engineering physics 24 (1) (1973) 43-48.

[138] M. Arik and A. Bar-Cohen. Ebullient cooling of integrated circuits by Novec fluids. in Intersociety Electronic Packaging Conf, Hawaii, USA. 2001

[139] M. J. Brusstar and H. Merte Jr, Effects of heater surface orientation on the critical heat flux—II. A model for pool and forced convection subcooled boiling, International Journal of Heat and Mass Transfer 40 (17) (1997) 4021-4030.

[140] J. Y. Chang and S. M. You, Heater Orientation Effects on Pool Boiling of Micro-Porous-Enhanced Surfaces in Saturated FC-72, Journal of Heat Transfer 118 (4) (1996) 937-943.

[141] Y. A. Kirchenko and P. S. Chernyakov, Determination of the first critical thermal flux on flat heaters, Journal of engineering physics 20 (6) (1971) 699-703.

[142] T. G. Theofanous and T.-N. Dinh, High heat flux boiling and burnout as microphysical phenomena: mounting evidence and opportunities, Multiphase Science and Technology 18 (3) (2006) 251-276.

[143] L. Liao, R. Bao, and Z. Liu, Compositive effects of orientation and contact angle on critical heat flux in pool boiling of water, Heat and Mass Transfer 44 (12) (2008) 1447-1453.

[144] M. M. Sarafraz and F. Hormozi, Convective boiling and particulate fouling of stabilized CuO-ethylene glycol nanofluids inside the annular heat exchanger, International Communications in Heat and Mass Transfer 53 (2014) 116-123.

[145] X. Yimin and L. Qiang, Heat transfer enhancement of nanofluids, International Journal of Heat and Fluid Flow 21 (1) (2000) 58-64.

[146] M. I. Pryazhnikov, A. V. Minakov, V. Y. Rudyak, and D. V. Guzei, Thermal conductivity measurements of nanofluids, International Journal of Heat and Mass Transfer 104 (2017) 1275-1282.

[147] M. Lattuada, P. Sandkühler, H. Wu, J. Sefcik, and M. Morbidelli, Aggregation kinetics of polymer colloids in reaction limited regime: experiments and simulations, Advances in Colloid and Interface Science 103 (1) (2003) 33.

[148] H. Uchikawa, S. Hanehara, and D. Sawaki, The Role of Steric Repulsive Force in the Dispersion of Cement Particles in Fresh Paste Prepared with Organic Admixture, Cement and Concrete Research 27 (1) (1997) 37-50.

[149] N. A. C. Sidik, H. A. Mohammed, O. A. Alawi, and S. Samion, A Review on Preparation Methods and Challenges of Nanofluids, International Communications in Heat and Mass Transfer 54 (2014) 115-125.

[150] M. Karimzadehkhouei, M. Shojaeian, K. Sendur, M. P. Mengüç, and A. Kosar, The effect of nanoparticle type and nanoparticle mass fraction on heat transfer enhancement in pool boiling, International Journal of Heat and Mass Transfer 109 (2017) 157-166.

[151] V. Kumar, A. K. Tiwari, and S. K. Ghosh, Characterization and Performance of Nanofluids in Plate Heat Exchanger, Materials Today: Proceedings 4 (2017) 4070-4078.

[152] F. Yu, Y. Chen, X. Liang, J. Xu, C. Lee, Q. Liang, P. Tao, and T. Deng, Dispersion stability of thermal nanofluids, Progress in Natural Science: Materials International 27 (2017) 531-542.

[153] M. Kole and T. K. Dey, Thermophysical and pool boiling characteristics of ZnO-ethylene glycol nanofluids, International Journal of Thermal Sciences 62 (2012) 61-70.

[154] Y. Wei, X. Huawing, C. Lifei, and L. Yang, Enhancement of thermal conductivity of kerosene-based Fe_3O_4 nanofluids prepared via phase-transfer method, Colloids and Surfaces A: Physiochemical and Engineering Aspects 355 (2010) 109-113.